A fingerprint of surface-tension anisotropy in the free-energy cost of nucleation

Santi Prestipino, Alessandro Laio, and Erio Tosatti

Additional information on J. Chem. Phys.

A fingerprint of surface-tension anisotropy in the free-energy cost of nucleation

Santi Prestipino,[1,a)] Alessandro Laio,[2,b)] and Erio Tosatti[2,3,c)]

[1]*Università degli Studi di Messina, Dipartimento di Fisica e di Scienze della Terra, Contrada Papardo, I-98166 Messina, Italy*
[2]*International School for Advanced Studies (SISSA) and UOS Democritos, CNR-IOM, Via Bonomea 265, I-34136 Trieste, Italy*
[3]*The Abdus Salam International Centre for Theoretical Physics (ICTP), P.O. Box 586, I-34151 Trieste, Italy*

We focus on the Gibbs free energy ΔG for nucleating a droplet of the stable phase (e.g., solid) inside the metastable parent phase (e.g., liquid), close to the first-order transition temperature. This quantity is central to the theory of homogeneous nucleation, since it superintends the nucleation rate. We recently introduced a field theory describing the dependence of ΔG on the droplet volume V, taking into account besides the microscopic fuzziness of the droplet-parent interface, also small fluctuations around the spherical shape whose effect, assuming isotropy, was found to be a characteristic logarithmic term. Here we extend this theory, introducing the effect of anisotropy in the surface tension, and show that in the limit of strong anisotropy $\Delta G(V)$ once more develops a term logarithmic on V, now with a prefactor of opposite sign with respect to the isotropic case. Based on this result, we argue that the geometrical shape that large solid nuclei mostly prefer could be inferred from the prefactor of the logarithmic term in the droplet free energy, as determined from the optimization of its near-coexistence profile. © *2013 American Institute of Physics*. [http://dx.doi.org/10.1063/1.4790635]

I. INTRODUCTION

When a homogeneous, defect-free bulk system is brought across a first-order phase boundary, it may survive in its metastable state even for a long time, until the stable phase spontaneously nucleates.[1,2] The nucleation process has attracted much attention over the years, both from a fundamental point of view as well as for its great practical interest. To mention but one example, a better control of crystal nucleation in protein solutions could help hinder protein condensation which is at the heart of several human pathologies.[3] Thermal fluctuations continuously sprout droplets of the stable phase inside the metastable mother phase. Small droplets dissolve, for the gain in volume free energy fails to compensate the loss in surface free energy. Occasionally, a droplet is sufficiently large that it is favorable for it to grow. Once this happens, the solid nucleus expands until the whole liquid crystallizes. Quenching the system deeper and deeper lowers the nucleation barrier until the point where the barrier vanishes (kinetic spinodal limit). Beyond this threshold, nucleation ceases and the phase transition occurs through spinodal decomposition and coarsening (i.e., uniformly throughout the material). Classical nucleation theory (CNT)[4–6] provides the simplest theoretical framework in which the initial stage of the phase transformation can be described. In this theory, an isolated droplet is schematized, regardless of its size, as a sphere of bulk solid, separated from the liquid by a sharp interface with a constant free-energy cost per unit area σ ("capillarity approximation"). This gives rise to a (Gibbs) free-energy difference between the supercooled liquid system with and without a solid cluster, that is

$$\Delta G(V) = -\rho_s|\Delta\mu|V + (36\pi)^{1/3}\sigma V^{2/3}, \qquad (1.1)$$

where V is the cluster volume, $\Delta\mu < 0$ is the difference in chemical potential between solid and liquid, and ρ_s is the bulk-solid number density. The droplet grows if it exceeds a critical size V^* corresponding to the maximum $\Delta G (\equiv\Delta G^*)$, which thus provides the activation barrier to nucleation.[7]

The cluster free energy $\Delta G(V)$ can be accessed numerically via the statistics of cluster size, through which the validity of Eq. (1.1) for specific model interactions can be directly tested. We recently showed[8] that the accuracy of CNT is less than satisfactory in estimating the size probability distribution of clusters, especially the smaller ones, implying that interface-tension estimates based on the use of CNT are systematically in error. We then proposed a more detailed field theory of the nucleation barrier, based on the assumption that clusters are soft and not sharp, and can deviate mildly from the spherical shape ("quasispherical" approximation). If the solid-liquid interface tension is taken to be isotropic, the volume dependence of the Gibbs free energy of a cluster is of the Dillmann-Meier form,[9]

$$\Delta G(V) = -\rho_s|\Delta\mu|V + AV^{2/3} + BV^{1/3} + C - \frac{7}{9}k_B T \ln\frac{V}{a^3}, \qquad (1.2)$$

where A, B, and C can all be expressed as explicit functions of the "microscopic" parameters entering a Landau free energy, and a is a microscopic length. It turned out that the numerical

profiles of ΔG in a few test cases and at various supersaturations are better reproduced by this theory.

Here we critically reconsider the most severe assumption made in that derivation, namely the isotropy of the solid-liquid interface tension. We show that the theory introduced in Ref. 8 can be extended relaxing this important approximation, and that the results change. Starting once again from a Landau-like theory, we derive an interface Hamiltonian, that allows estimating the probability of observing a cluster of any shape and size. The angular dependence of the interface tension is taken into account by terms that depend on the local orientation of the cluster surface. Within this framework, we calculate $\Delta G(V)$ in the limit of strong surface anisotropy and compare it with the isotropic case. For large anisotropy, the cluster free energy still retains at large size a logarithmic term, however, with a prefactor of opposite sign to the isotropic one. On account of this, we suggest that the nominal shape of large solid nuclei could be guessed from the optimization of the actual $\Delta G(V)$ close to coexistence. Looking for a numerical exemplification, we conducted 3D Monte Carlo simulations of the Ising model extracting $\Delta G(V)$ for clusters of variable size V, at various distances from coexistence. Although we could not really attain sizes where the anisotropic shape effects are heavy, we do detect evidence that the sign is as expected for large anisotropy.

The paper is organized as follows. We start in Sec. II by relaxing the approximation of an infinitely sharp cluster interface, with the introduction of a Landau free energy. From that, an effective sharp-interface Hamiltonian is derived in Sec. III, as an intermediate step to building up a field theory for isotropic surfaces where small shape fluctuations are allowed (Sec. IV A). Eventually, this leads to a modified-CNT expression of $\Delta G(V)$. In Sec. IV B, the issue of interface anisotropies is addressed, and we show by examples how the dependence of the interface free energy on the local surface normal affects the formation energy of a large cluster. Next, in Sec. V, we check our theory against old and fresh Monte Carlo simulation data for the nucleation barrier to magnetization reversal in the 3D Ising model above the roughening temperature. While confirming that CNT is not generally adequate to fit the numerical $\Delta G(V)$ data, this analysis also gives a quantitative measure of the errors made with CNT and demonstrates their cancellation in the more general theory. Finally, our conclusions are presented in Sec. VI.

II. DIFFUSE INTERFACE: LANDAU THEORY

The main assumption behind CNT is that of a sharp and spherical cluster surface. A way to relax this approximation is through the introduction of a scalar, non-conserved order-parameter (OP) field $\phi(\mathbf{x})$ ("crystallinity") which varies smoothly from one phase to the other. Hence, the solid-liquid interface becomes diffuse in space, even though only on a microscopic scale. In practice, ϕ may be thought of as the local value of the main Fourier coefficients of the crystal-periodic one-body density $n(\mathbf{x})$, i.e., those relative to the reciprocal-lattice vectors which are closest in modulus to the point where the liquid structure factor reaches its maximum.[10] Otherwise, ϕ may be identified with the parameter discriminating be-

tween solid and liquid in an ansatz like

$$n(\mathbf{x}) = \left(\frac{\phi}{\pi}\right)^{3/2} \sum_{\mathbf{R}} e^{-\phi(\mathbf{x}-\mathbf{R})^2} = \rho_s \sum_{\mathbf{G}} e^{-G^2/(4\phi)} e^{i\mathbf{G}\cdot\mathbf{x}} \quad (2.1)$$

assuming a specific crystal symmetry and an overall number density ρ_s.

Across the solid-liquid interface, ϕ is no longer constant and, for a system with short-range forces, the thermodynamic cost of the interface may be described through the free-energy functional[11–15]

$$\mathcal{G}[\phi; \hat{\mathbf{n}}] = \int d^3x \left\{ \frac{c(\hat{\mathbf{n}})}{2}(\nabla\phi)^2 + \frac{\kappa(\hat{\mathbf{n}})}{2}(\nabla^2\phi)^2 + g(\phi(\mathbf{x})) \right\}, \quad (2.2)$$

where $c, \kappa > 0$ are stiffness parameters dependent on the interface orientation as defined by the unit normal $\hat{\mathbf{n}}$ and $g(\phi)$ is the specific Landau free energy of the homogeneous system, taken the bulk liquid as a reference. In Eq. (2.2), besides the customary square-gradient term, also a square-laplacian term appears. This is the next-to-leading isotropic term in the gradient expansion of the Landau free-energy density.[16] Even though being a fourth-order gradient term, it is, however, only second-order in the order parameter, and this places it on the same footing as the square-gradient term (hence, potentially relevant). We shall see below that, without such a term, the bending rigidity (i.e., the coefficient of H^2 in Eq. (3.15) below) would simply be zero. Below the melting temperature T_m, g shows, besides the liquid minimum, also a second and deeper solid minimum. Exactly at coexistence, the two minima are equal, falling at $\phi_- = \phi_{s0}$ in the bulk solid and at $\phi_+ = 0$ in the bulk liquid, which means that $g(\phi_{s0}) = g(0) = 0$ while $g(\phi) > 0$ otherwise.

When boundary conditions are applied such that $\phi \to \phi_\pm$ for $z \to \pm\infty$, a planar interface orthogonal to z is forced to appear in the system. The corresponding OP profile is the stationary solution $\phi_0(z; \hat{\mathbf{n}})$ of (2.2) that satisfies the boundary conditions

$$c(\hat{\mathbf{n}})\phi_0'' - \kappa(\hat{\mathbf{n}})\phi_0'''' = \frac{dg}{d\phi}(\phi_0; T = T_m), \quad \text{with } \phi_0(-\infty) = \phi_{s0}$$

$$\text{and } \phi_0(+\infty) = 0. \quad (2.3)$$

From now on, we simplify the notation by dropping any reference to $\hat{\mathbf{n}}$ in c, κ, and ϕ_0. Equation (2.3) can be simplified by multiplying both sides by $\phi_0'(z)$ and integrating by parts. We thus arrive at a new boundary value problem

$$\kappa\phi_0'\phi_0''' = \frac{c}{2}\phi_0'^2 + \frac{\kappa}{2}\phi_0''^2 - g(\phi_0), \quad \text{with } \phi_0(-\infty) = \phi_{s0}$$

$$\text{and } \phi_0(+\infty) = 0. \quad (2.4)$$

Obviously, $\mathcal{G}[\phi_0]$ represents the free-energy cost of the interface at $T = T_m$.

At temperature below coexistence, the absolute minimum of $g(\phi)$ falls at $\phi = \phi_s > 0$ for $\Delta T \equiv T - T_m < 0$. This can be described by

$$g(\phi) = c_2\phi^2 + c_3\phi^3 + c_4\phi^4 + \dots \quad (2.5)$$

with $c_2 = c_{20} + c'_{20}\Delta T$ ($c_{20}, c'_{20} > 0$), all other c_n coefficients being constant.

For the remaining part of this section, we will assume that c and κ do not depend on $\hat{\mathbf{n}}$. Under this condition, a large solid cluster can be assumed to be spherical, with a OP profile described by $\phi_0(r - R)$,[13] provided the center of $\phi_0(z)$ is at $z = 0$. From this ansatz, in Ref. 8 we derived an expression for the cluster free energy,

$$\Delta G(R) = 4\pi R^2 \sigma^{\mathrm{L}} \left(1 - \frac{2\delta^{\mathrm{L}}}{R} + \frac{\epsilon^{\mathrm{L}}}{R^2} \right) - \frac{4}{3}\pi R^3 \rho_s |\Delta\mu| \tag{2.6}$$

in terms of quantities ($\sigma^{\mathrm{L}}, \delta^{\mathrm{L}}, \epsilon^{\mathrm{L}}$) which depend linearly on the supersaturation $|\Delta\mu| \propto |\Delta T|$. Equation (2.6) resembles the CNT expression, Eq. (1.1), with the crucial difference that the interface free energy is now a function of both R and T:

$$\sigma(R; T) = \sigma^{\mathrm{L}} \left(1 - \frac{2\delta^{\mathrm{L}}}{R} + \frac{\epsilon^{\mathrm{L}}}{R^2} \right). \tag{2.7}$$

Exactly of this form is the tension of the equilibrium interface between a liquid droplet and the vapour background in the Lennard-Jones model, as being extracted from the particle-number histogram in grand-canonical simulations of samples of increasing size.[17] At coexistence, the solid-liquid interface tension and the Tolman length[18] are given by

$$\sigma_m \equiv \sigma^{\mathrm{L}}(T_m) = \int_{-\infty}^{+\infty} \mathrm{d}z \left[c\phi_0'^2(z) + 2\kappa\phi_0''^2(z) \right],$$
$$\delta_m \equiv \delta^{\mathrm{L}}(T_m) = -\frac{\int_{-\infty}^{+\infty} \mathrm{d}z\, z \left[c\phi_0'^2(z) + 2\kappa\phi_0''^2(z) \right]}{\int_{-\infty}^{+\infty} \mathrm{d}z \left[c\phi_0'^2(z) + 2\kappa\phi_0''^2(z) \right]}. \tag{2.8}$$

A nonzero δ_m occurs if and when $\phi_0(z)$ is *asymmetric* around zero, as is generally the case for the interface between phases of a different nature (see Appendix A). Summing up, Eq. (2.6) describes the corrections to CNT which arise by replacing the assumption of a sharp solid-liquid interface with a more realistic finite width, in the case of isotropic surface tension and Tolman length.

III. SHAPE FLUCTUATIONS: THE INTERFACE HAMILTONIAN

A real cluster may be spherical only on average. Far from being static, clusters fluctuate widely away from their mean shape.[19,20] To describe fluctuations, we switch from a description in terms of the crystallinity OP to another in which the cluster shape itself rises to the role of fundamental variable. We begin by deriving a coarse-grained, purely geometrical Hamiltonian for the cluster surface directly from the mi-

croscopic free-energy functional (2.2), under the assumption of small deviations of the interface from planarity. The outcome is a Canham-Helfrich (CH) Hamiltonian,[21,22] containing spontaneous-curvature and bending penalty terms in addition to interface tension.

For the present derivation, we build on Refs. 23 and 24. Other attempts to derive an effective interface Hamiltonian from a mean-field density functional are described in Refs. 25 and 26. Let the cluster "surface" be depicted as a closed mathematical surface Σ embedded in three-dimensional space and let $\mathbf{R}(u, v)$ be the parametrization (coordinate patch) of an infinitesimal piece of Σ. We switch from 3D cartesian coordinates, $\mathbf{r} = (x, y, z)$, to new coordinates $q_\alpha = (u, v, \zeta)$ (tangential and normal to Σ) by the transformation

$$\mathbf{r} = \mathbf{R}(u, v) + \zeta\hat{\mathbf{n}}(u, v), \tag{3.1}$$

where

$$\hat{\mathbf{n}}(u, v) = \frac{\mathbf{R}_u \wedge \mathbf{R}_v}{|\mathbf{R}_u \wedge \mathbf{R}_v|} \tag{3.2}$$

is the unit normal to Σ. For a patch that deviates only slightly from planarity, we may adopt a free energy $\mathcal{G}[\phi_0(\zeta(x, y, z))]$, thus arriving at the surface Hamiltonian

$$\mathcal{H}_s[\Sigma] = \int \mathrm{d}u\, \mathrm{d}v\, \mathrm{d}\zeta\, J \left\{ \frac{c}{2}(\nabla\phi_0(\zeta))^2 + \frac{\kappa}{2}(\nabla^2\phi_0(\zeta))^2 + g(\phi_0(\zeta)) \right\} \tag{3.3}$$

with $J = |\mathbf{r}_u \cdot (\mathbf{r}_v \wedge \mathbf{r}_\zeta)| = |\hat{\mathbf{n}} \cdot (\mathbf{r}_u \wedge \mathbf{r}_v)|$. In order to make Eq. (3.3) simpler, it is convenient to view the patch as parametrized in terms of orthonormal, arc-length coordinates, i.e., $\mathbf{R}_u \cdot \mathbf{R}_v = 0$ and $|\mathbf{R}_u| = |\mathbf{R}_v| = 1$ all over the patch. Although this construction is rigorously possible only for surfaces having zero Gaussian curvature ($K = 0$),[27] we can reasonably expect that only small errors of order K are made for quasiplanar interfaces. With this caution in mind, we go on to get (see Appendix B):

$$\frac{\partial\mathbf{r}}{\partial u} = \left(1 - \zeta\kappa_n^{(1)}\right)\mathbf{R}_u - \zeta\tau_g\mathbf{R}_v,$$
$$\frac{\partial\mathbf{r}}{\partial v} = -\zeta\tau_g\mathbf{R}_u + \left(1 - \zeta\kappa_n^{(2)}\right)\mathbf{R}_v, \tag{3.4}$$
$$\frac{\partial\mathbf{r}}{\partial\zeta} = \hat{\mathbf{n}},$$

where $\kappa_n^{(1)}$ and $\kappa_n^{(2)}$ are the normal curvatures of the u- and v-lines, respectively, and $\tau_g \equiv \tau_g^{(1)} = -\tau_g^{(2)}$ is the geodetic torsion. From Eqs. (3.4), we readily derive the metric tensor $g_{\alpha\beta}$,

$$g_{\alpha\beta} \equiv \frac{\partial\mathbf{r}}{\partial q_\alpha} \cdot \frac{\partial\mathbf{r}}{\partial q_\beta} = \begin{pmatrix} \left(1 - \zeta\kappa_n^{(1)}\right)^2 + \zeta^2\tau_g^2 & -2\zeta\tau_g + \zeta^2\tau_g\left(\kappa_n^{(1)} + \kappa_n^{(2)}\right) & 0 \\ -2\zeta\tau_g + \zeta^2\tau_g\left(\kappa_n^{(1)} + \kappa_n^{(2)}\right) & \left(1 - \zeta\kappa_n^{(2)}\right)^2 + \zeta^2\tau_g^2 & 0 \\ 0 & 0 & 1 \end{pmatrix} \tag{3.5}$$

and the Jacobian,

$$J = \left(1 - \zeta \kappa_n^{(1)}\right)\left(1 - \zeta \kappa_n^{(2)}\right) - \zeta^2 \tau_g^2 = \sqrt{g} \qquad (3.6)$$

g being the determinant of (3.5). Considering that covariant and contravariant components of a vector are built by projecting it on the bases ∇q_α and $\partial \mathbf{r}/\partial q_\alpha$, respectively, we can calculate the gradient of a scalar field ϕ and the divergence of a vector field $\mathbf{A}$ in local coordinates as follows:

$$\nabla\phi = \frac{\partial\phi}{\partial q_\alpha} g^{\alpha\beta} \frac{\partial\mathbf{r}}{\partial q_\beta} \quad \text{and} \quad \nabla\cdot\mathbf{A} = \frac{1}{\sqrt{g}}\frac{\partial}{\partial q_\alpha}(\sqrt{g} A^\alpha),$$

$$(3.7)$$

$g^{\alpha\beta}$ being the inverse of (3.5). In particular,

$$\nabla\phi(\zeta) = \phi'(\zeta)\widehat{\mathbf{n}} \quad \text{and} \quad \nabla^2\phi(\zeta) = \phi''(\zeta) + \phi'(\zeta)\nabla\cdot\widehat{\mathbf{n}},$$

$$(3.8)$$

where

$$\nabla\cdot\widehat{\mathbf{n}} = \frac{1}{\sqrt{g}}\left(-\kappa_n^{(1)} - \kappa_n^{(2)} - 2\zeta\tau_g^2\right). \qquad (3.9)$$

Finally, the mean and Gaussian curvatures of the patch are given by

$$H = \frac{1}{2}\nabla\cdot\widehat{\mathbf{n}}\bigg|_{\zeta=0} = -\frac{1}{2}\left(\kappa_n^{(1)} + \kappa_n^{(2)}\right) \qquad (3.10)$$

and

$$K = \widehat{\mathbf{n}}\cdot\left(\frac{\partial\widehat{\mathbf{n}}}{\partial u} \wedge \frac{\partial\widehat{\mathbf{n}}}{\partial v}\right) = \kappa_n^{(1)}\kappa_n^{(2)} - \tau_g^2. \qquad (3.11)$$

Hence, (1) the mean curvature, which is defined only up to a sign depending on our convention on the orientation of $\widehat{\mathbf{n}}$, is half the sum of the two normal curvatures relative to any orthogonal parametrization, i.e., not necessarily the two principal curvatures; (2) since K is the product of the two principal curvatures, the geodetic torsion must vanish when the coordinate lines are also lines of curvature.

We are now in a position to simplify Eq. (3.3). Upon using Eq. (2.4) to eliminate $g(\phi_0)$ in favor of $(c/2)\phi_0'^2 + (3\kappa/2)\phi_0''^2 - \kappa(\phi_0'\phi_0'')'$, and inserting Eqs. (3.6), (3.8), (3.10), and (3.11) we eventually get

$$\mathcal{H}_s = \int du\, dv\, d\zeta\, (1 + 2\zeta H + \zeta^2 K)\left\{ c\phi_0'^2(\zeta) + \frac{3}{2}\kappa\phi_0''^2(\zeta) \right.$$

$$+ \frac{\kappa}{2}\left(\phi_0''(\zeta) + \phi_0'(\zeta)\frac{2H - 2\zeta\tau_g^2}{1 + 2\zeta H + \zeta^2 K}\right)^2$$

$$\left. -\kappa(\phi_0'(\zeta)\phi_0''(\zeta))' \right\}.$$

$$(3.12)$$

We now argue that, to a first approximation, any term of order higher than H^2 and K can be discarded. Moreover, $\int du\,dv = \int dS$ since $|\mathbf{R}_u \wedge \mathbf{R}_v| = 1$. Finally, the geodetic torsion vanishes if we perform a change of integration variables (that is, a change of parametrization) such that the coordinate lines are also lines of curvature.[28] In the end, we are left with the

classic Canham-Helfrich Hamiltonian for fluid membranes

$$\mathcal{H}_s = \int_\Sigma dS\, (\overline{a} + \overline{b}H + \overline{c}H^2 + \overline{d}K), \qquad (3.13)$$

with the following explicit expressions for the coefficients:

$$\overline{a} = \int_{-\infty}^{+\infty} d\zeta\, \left[c\phi_0'^2(\zeta) + 2\kappa\phi_0''^2(\zeta)\right],$$

$$\overline{b} = 2\int_{-\infty}^{+\infty} d\zeta\, \zeta\left[c\phi_0'^2(\zeta) + 2\kappa\phi_0''^2(\zeta)\right],$$

$$(3.14)$$

$$\overline{c} = 2\kappa\int_{-\infty}^{+\infty} d\zeta\, \phi_0'^2(\zeta),$$

$$\overline{d} = \int_{-\infty}^{+\infty} d\zeta\, \left\{\zeta^2\left[c\phi_0'^2(\zeta) + 2\kappa\phi_0''^2(\zeta)\right] - \kappa\phi_0'^2(\zeta)\right\}.$$

A few remarks are now in order: (1) H and K are reparametrization invariants, hence no ambiguity arises from the arbitrariness of the parametrization used. (2) The above derivation actually applies for just one Σ patch. However, upon viewing Σ as the union of many disjoint patches, the Hamiltonian (3.13) holds for the whole Σ as well. (3) As anticipated, the coefficient $\overline{d}$ of the K term in (3.13) could be different from the quoted one since a parametrization in terms of orthonormal coordinates does not generally exist. However, as far as we only allow for clusters with the topology of a sphere, $\int_\Sigma dS\, K$ takes the constant value of 4π by the Gauss-Bonnet theorem and the K term in $\mathcal{H}_s$ can be dropped. Upon comparing the definition of $\overline{a}$ and $\overline{b}$ in Eqs. (3.14) with Eqs. (2.8), we can rewrite Eq. (3.13) in the form (restoring everywhere the dependence upon interface orientation):

$$\mathcal{H}_s = \int_\Sigma dS\, (\sigma_m(\widehat{\mathbf{n}}) - 2\sigma_m(\widehat{\mathbf{n}})\delta_m(\widehat{\mathbf{n}})H + 2\lambda(\widehat{\mathbf{n}})H^2),$$

$$(3.15)$$

where $\lambda = \overline{c}/2$ (we note that $\lambda = \kappa\phi_{s0}^2/(3\ell)$ under the same hypotheses for which Eq. (A15) holds). (4) The term linear in H is related to the *spontaneous curvature* of Σ, $H_0 = -\overline{b}/(2\overline{c})$, which is proportional to the Tolman length δ_m. A nonzero value of H_0 yields a difference in energy between inward and outward interface protrusions, thus entailing a nonzero δ_m. The additional fact that in systems, such as the Ising model, where the symmetry is perfect between the two phases then $\delta_m = 0$, has long been known.[13]

We point out that Eq. (3.15) retains the same form as in the isotropic case.[8] In the general anisotropic case, the dependence of the Hamiltonian parameters on the interface normal is through the constants c and κ, and the function $\phi_0(z)$.

IV. THE CLUSTER FREE ENERGY IN TWO EXTREME CASES: ISOTROPIC AND STRONGLY ANISOTROPIC INTERFACE TENSION

Considering that every single realization of the profile of the cluster surface should be sampled in equilibrium with a weight proportional to $\exp\{-\beta\mathcal{H}_s\}$, it is natural to define a

volume-dependent cost of cluster formation through

$$\Delta G(V) = -\rho_s |\Delta\mu| V + F_s(V) \qquad (4.1)$$

with

$$
\begin{aligned}
F_s(V) &= -k_B T \ln Z_s(V) \\
&= -k_B T \ln \left\{ a^3 \int \mathcal{D}\Sigma\, e^{-\beta\mathcal{H}_s}\, \delta(\mathcal{V}[\Sigma] - V) \right\} \quad (4.2)
\end{aligned}
$$

In the above expression of the constrained partition function Z_s, $a = \rho_s^{-1/3}$ is a microscopic length of the system, $\mathcal{V}[\Sigma]$ is the volume enclosed by the closed surface Σ, and $\mathcal{D}\Sigma$ a yet-to-be-specified integral measure.

While the calculation of F_s for a realistic form of $\hat{\mathbf{n}}$-dependent parameters in (3.15) is certainly possible numerically once the admissible surfaces have been parametrized in terms of a basis of eigenfunctions, some restrictions are to be made in practice if we want to make analytical progress. In the following, we examine two limiting cases for $\sigma_m(\hat{\mathbf{n}})$, according to whether it is constant or strongly anisotropic. In general, a strongly anisotropic σ_m is typical of e.g. systems where melting is very strongly first order, implying very sharp and thus direction dependent solid-liquid interfaces, such as for example in the case of alkali halides.[29] That brings about a non-spherical cluster shape through the prescription that the surface free energy be the minimum possible for the given cluster volume V. The same condition is responsible for a spherical shape when the interface free energy is isotropic.

A. Isotropic interfaces

If σ_m, δ_m, and λ in Eq. (3.15) do not depend on $\hat{\mathbf{n}}$, the shape of a cluster is on average spherical. We here compute the free energy (4.2) assuming small deviations from this shape.

Neglecting overhangs and liquid inclusions, let $r = R(\theta, \phi)$ be the equation of Σ in spherical coordinates. We assume only small deviations from a sphere, i.e., $R(\theta, \phi) = R_0[1 + \epsilon(\theta, \phi)]$, with $\epsilon(\theta, \phi) \ll 1$.[30] Then, we expand $\epsilon(\theta, \phi)$ in real spherical harmonics,

$$\epsilon(\theta, \phi) = \sum_{l=1}^{\infty} \sum_{m=-l}^{l} x_{l,m} Y_{l,m}(\theta, \phi) \qquad (4.3)$$

and we agree to ignore, from now on, all terms beyond second-order in the coefficients $x_{l,m}$. With these specifications, we obtain approximate expressions for the area of Σ and its enclosed volume, as well as for the mean curvature H. Upon inserting this form of $\mathcal{H}_s$ in terms of the $x_{l,m}$ into Eq. (4.2), we are left with the evaluation of a Gaussian integral. While we refer the reader to Appendix C for all the technicalities, we here quote the result of the calculation. The

free energy cost of cluster formation for large V is

$$
\begin{aligned}
\Delta G(V) = {}& -\rho_s |\Delta\mu| V + (36\pi)^{1/3} \sigma^{\text{QS}} V^{2/3} \\
& - (384\pi^2)^{1/3} \sigma^{\text{QS}} \delta^{\text{QS}} V^{1/3} \\
& + 4\pi \sigma^{\text{QS}} \epsilon^{\text{QS}} - \frac{7}{6} k_B T \ln\left((36\pi)^{1/3} \left(\frac{V}{a^3}\right)^{2/3} \right),
\end{aligned}
$$
$$(4.4)$$

where σ^{QS}, δ^{QS}, and ϵ^{QS} can be read in Eq. (C21). The above formula is strictly valid only near coexistence, where the various assumptions beneath its derivation are expected to hold true. We have thus found that the surface free energy has a form consistent with the Dillmann-Meier ansatz, with T-dependent parameters σ^{QS}, δ^{QS}, and ϵ^{QS} that are different (even at T_m!) from the corresponding ones in Landau-theory σ^{L}, δ^{L}, and ϵ^{L}, and with a universal logarithmic correction to the mean-field form of ΔG. This term is responsible for the well known $R^{*7/3}$ exponential prefactor to the nucleation rate.[31]

B. Anisotropic interfaces

We now consider an interface tension of the form

$$\sigma(\hat{\mathbf{n}}) = \sigma_{100}\left[1 + M\left(\hat{n}_x^4 + \hat{n}_y^4 + \hat{n}_z^4 - 1\right)^2\right] \qquad (4.5)$$

with $M \to \infty$, written in terms of the cartesian components of the outer normal to the cluster surface. In the infinite-M limit, the equilibrium crystal shape is a cube, though rectangular cuboids are also admissible, though not optimal, shapes (they arise at non-zero temperatures). The terms in Eq. (3.15) beyond the first are singular in the $M \to \infty$ limit; however, they would contribute to the surface free energy if M were large but not infinite, see more in Appendix D. In the same Appendix we show that the asymptotic, large-V free-energy cost of cluster formation is given by

$$
\begin{aligned}
\Delta G(V) = {}& -\rho_s |\Delta\mu| V + 6\sigma^{PP} V^{2/3} + 12\nu^{PP} V^{1/3} \\
& + k_B T \ln\left(6\left(\frac{V}{a^3}\right)^{2/3} \right) + \text{const} \qquad (4.6)
\end{aligned}
$$

with $\sigma^{PP} \equiv \sigma_{100}$. Similarly to the isotropic case, in the cluster free energy (4.6) both a logarithmic term and an offset are added to the classical CNT expression of ΔG for a cubic cluster of side $V^{1/3}$. The Tolman term in Eq. (4.6) only appears if we envisage an energy penalty, that is ν^{PP} per unit length, also for the edges.

More generally, in all the anisotropic-nucleation models examined in Appendix D, the consideration of clusters of same type but unequal edges/semiaxes provides for "breathing" fluctuations of the surface that determine the appearance of a logarithmic term in ΔG. In fact, for all such models, the analytically computed $\Delta G(V)$ is asymptotically given, as in Eq. (4.6), by the CNT expression – as written for the respective symmetric shape – plus subleading terms in the form of a Tolman term, a universal logarithm ($c k_B T \ln V^{(d-1)/d}$ in d dimensions), and a negative offset. The value of c is 1/2 for rectangles and 1 for both cuboids and ellipsoids. This is to be contrasted with the quasispherical-cluster case, where

$c = -7/6$ by Eq. (4.4). Apparently, the value of c is sensitive to both the space dimensionality and the number of independent parameters that are needed to describe the cluster shape, in turn crucial to determine the entropy contents of the surface degrees of freedom (for a quasispherical cluster, this number of parameters goes to infinity with V). In short, a large anisotropy in the interface tension has the overall effect of drastically reducing the spectrum of thermal fluctuations of cluster shape. The reduction cancels the entropy gain which these fluctuations produced in the isotropic case.

This attractive prediction is a difficult one to fully validate numerically at present. A logarithmic correction to CNT can only be detected if we push the numerical investigation of $\Delta G(V)$ so close to coexistence as to make the Dillmann-Meier form exact for all but the smallest clusters, and that is still a difficult task (see more in Sec. V). In the near future, with faster computers becoming available, we can imagine that it will be possible to directly probe the cluster geometry through the optimization of the logarithmic prefactor in an ansatz of the kind (4.4) or (4.6), and thus choose among the many cluster models in the market, the one which is most appropriate to the problem at hand.

V. NUMERICAL ASSESSMENT OF THE THEORY

We now critically consider if there are signatures of the degree of anisotropy of the interface free energy in the free-energy cost of cluster formation for a specific instance of microscopic interaction.

We first recall how the work of formation of a n-particle cluster is calculated from simulations.[32–34] Given a criterion to identify solid-like clusters within a predominantly liquid system of N particles, the average number of n-clusters is given, for $1 \ll n \simeq n*$, by $N_n = N e^{-\beta(G_n - n\mu_l)}$, where μ_l is the chemical potential of the liquid and G_n is the $\mathcal{O}(n)$ Gibbs free energy of the n-cluster, including also the contribution associated with the wiggling of the cluster center of mass within a cavity of volume V/N (observe that CNT estimates G_n as $n\mu_s + c\sigma(n/\rho_s)^{2/3}$, where μ_s is the chemical potential of the solid and c a geometrical factor). For rare clusters, it thus follows that $\Delta G(n) \equiv G_n - n\mu_l = -k_B T \ln(N_n/N)$. This equation is then taken to represent the work of cluster formation for all $n > 1$. Maibaum[35] has shown that the same formula applies for the Ising model.

However, for quenches that are not too deep, the spontaneous occurrence of a large solid cluster in the metastable liquid is a rare event. This poses a problem of poor statistics in the Monte Carlo (MC) estimation of N_n, which is overcome through, e.g., the use of a biasing potential that couples with the size $n_{\max}$ of the largest cluster. In practice, this keeps the system in the metastable state for all the n's of interest. By properly reweighting the sampled microstates one eventually recovers the ordinary ensemble averages. This umbrella-sampling (US) method was used in Refs. 32 and 36 to compute $\Delta G(n)$ for the Lennard-Jones fluid and the 3D Ising model, respectively. The main obstacle to the calculation of $\Delta G(n)$ by US is the necessity of performing the identification of the largest cluster in the system after every MC move. This problem can be somewhat mitigated by the use of a hybrid

MC algorithm,[37] which in our case reduced the simulation time by a factor of about 20.

A low-temperature Ising magnet where the majority of spins point against the applied field probably yields the simplest possible setup for the study of nucleation. Along the first-order transition line of the model, where two ("up" and "down") ferromagnetic phases coexist, the interface (say, (100)) between the two phases undergoes a roughening transition at a certain $T = T_R$. The up-down interface tension at coexistence is strongly anisotropic close to zero temperature; moreover, it is either singular or smooth according to whether T is below or above T_R. Strictly speaking, the interface tension is anisotropic also above T_R, though less and less so when approaching the critical temperature T_c from below.[38, 39] Exactly at T_c the interface tension critically vanishes.[40] When a sample originally prepared in the "down" phase is slightly pushed away from coexistence by a small positive field and thus made metastable, the critical droplet of the "up" phase is expected to be less and less spherical as T decreases.

With the 3D Ising model as a test system, we carried out a series of extensive US simulations, computing the cluster free energy $\Delta G(n)$ relative to the nucleation process of magnetization reversal for a fixed $T = 0.6 T_c$, slightly above the roughening temperature T_R of the (100) facet ($T_R = 0.5438\ldots T_c$[41]), and for a number of values of the external field h (0.30, 0.35, ..., 0.65, in J units). Two up spins are said to belong to the same cluster if there is a sequence of neighboring up spins between them; the counting of clusters was done with the Hoshen-Kopelman algorithm.[42] The absolute value of $\Delta G(1)$ was determined through a standard MC simulation of the system with all spins down, with no bias imposed on the sampling of the equilibrium distribution. We point out that, at the chosen temperature, the Ising surface tension is barely anisotropic,[38] which would exclude a net preference for either the spherical or the cubic shape. Furthermore, we are sufficiently far away from T_c not to worry about the percolation transition of geometric clusters which was first described in Ref. 43. This event, which would invalidate the assumption (at the heart of the conventional picture of nucleation) of a dilute gas of clusters, is still far away here.

Coherently with the physical picture at the basis of our theory, we verified for all the h considered that clusters close to critical indeed contain the vast majority of up spins in the system. A sample of the critical cluster for $h = 0.30$ is shown in Fig. 1. Looking at this picture, it is hard to say whether this particular realization of the critical cluster resembles more a sphere or a cube. When moving to $h = 0$, a spherical shape is eventually preferred over the cube far above T_R, whereas the opposite occurs much below T_R.

In Fig. 2, the ratio $\sigma^I(n)$ of the surface free energy $F_s(n) = \Delta G(n) + |\Delta\mu|n$ to the area $S(n)$ of the cluster surface is reported as a function of $n^{-1/3}$, and the data are fit using the functions (4.4) and (4.6) (we stress that different expressions apply for $S(n)$ on the left and right panels of Fig. 2, i.e., $(36\pi)^{1/3}n^{2/3}$ and $6n^{2/3}$, respectively; accordingly, the spherical σ's would typically turn out a factor $6/(36\pi)^{1/3}$ larger than the cubic σ's). Both fits are based on three parameters, namely σ, δ, and ϵ, which enter in a different way in Eqs. (4.4) and (4.6). However, the dependence on n is similar for the two
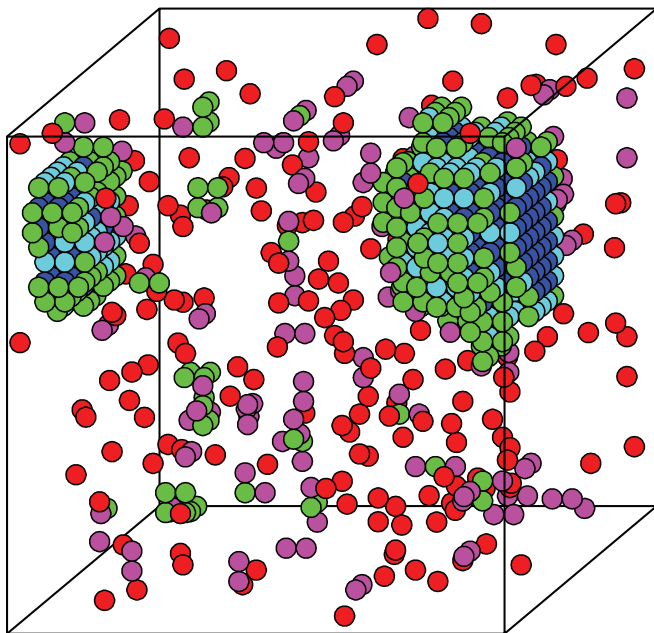
FIG. 1. A snapshot taken from our Monte Carlo simulation of the 3D Ising model at $T = 0.6 T_c$ and $h = 0.30$, showing a cluster of $n = 685$ up spins, i.e., close to the critical size for that h. Up spins are differently colored according to the number of nearest-neighboring up spins (blue, 6; cyan, 5; green, 2-4; magenta, 1; red, 0). Down spins are not shown.

fitting functions, except for the numerical factor in front of the (parameter-free) $n^{-2/3}\ln n$ term. Looking at Fig. 2, it appears that the quality of the "cubic" fit is slightly better than that of the "spherical" fit, in line with the fact that, for $T \gtrsim T_R$, the Ising surface tension is moderately anisotropic. Clearly, at $T = 0.6 T_c$ the nucleus is neither spherical nor cubic, and one may object that neither of the fits would actually be meaningful. We nonetheless argue that, within the uncertainty as-
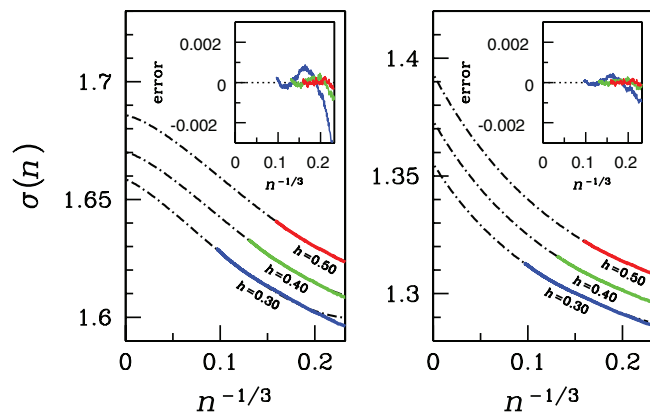

FIG. 2. The cluster free energy σ^I of the 3D Ising model on a cubic lattice in units of J/a^2 is plotted as a function of $n^{-1/3}$ (and up to $80^{-1/3}$) for three values of h and for $T = 0.6 T_c$ (a is the lattice spacing and $J > 0$ is the spin-coupling constant). The lattice includes 20^3 sites (25^3 for $h = 0.30$). Umbrella-sampling simulations consisted of 4M equilibrium sweeps for each n window (one window covering eleven values of n). Thick colored lines, MC data; black lines, least-square fits of the $n > 80$ data points for $h = 0.30$, 0.40, 0.50, based on Eqs. (4.4) (left) and (4.6) (right). Data plotted in the two panels look different simply because the expressions of cluster area $S(n)$ are different between left and right (see text). Inset: The difference between the raw data and the fit.

sociated with the finite h value in the simulations, the better one of the fits will correspond to the regular shape which is closest to that of the real nucleus, thus giving a qualitative indication of the prevailing isotropic or anisotropic character of the solid-liquid interface tension. When going to smaller and smaller h, and provided T is sufficiently above T_R, we expect that the "spherical" fit would eventually become better than the "cubic" fit.

VI. CONCLUSIONS

In order to estimate from nucleation the solid-liquid interface free energy σ_m of a substance, two indirect routes are available: one is through the measurement of the solid nucleation rate as a function of temperature (see, e.g., Refs. 46–48), the other is via the free energy ΔG of solid-cluster formation in a supercooled-liquid host, as determined for example in a numerical simulation experiment for a system model. In both cases, the theoretical framework of CNT has routinely been employed to extract σ_m. This is far from satisfactory, as discussed at length in Ref. 8 and in many other papers, due to the neglected cluster interface-tension dependence on both the droplet volume V and the supersaturation $|\Delta\mu|$.

Concentrating on the expression of the cluster formation energy ΔG as a function of V and $\Delta\mu$, we gave here an extension of the modified CNT theory first introduced in Ref. 8, now including anisotropy, which is important when only a few interface orientations survive in the equilibrium average cluster shape. We showed that, also in this case, a universal non-CNT $\ln V$ term is found in the asymptotic expression of the surface free energy versus volume, so long as an infinity of regular shapes is allowed to occur. However that term has now a different prefactor with respect to the quasispherical case. In particular, the sign is positive for large anisotropy and negative for vanishing anisotropy. The sign of that prefactor, which we surmise is related to the amount of surface entropy developed by cluster shape fluctuations, is proposed as the imprinted signature of the geometrical shapes most preferred by the nucleation cluster – negative for spherical or very isotropic shapes, positive for nearly polyhedric or anyway very anisotropic shapes. For the 3D Ising model slightly above the (100) roughening transition temperature, the detected sign suggests cubic rather than spherical cluster symmetry for moderate supersaturation/external field. Much more work and larger simulation sizes should be needed in the future in order to verify the expected change of sign of the $\ln V$ term as spherical shapes will be approached closer and closer to the coexistence line when the temperature is quite larger than T_R (though still far from the critical region).

ACKNOWLEDGMENTS

APPENDIX A: CALCULATION OF σ_m AND δ_m

In this Appendix, we provide approximate expressions for the quantities σ_m and δ_m in Eqs. (2.8) for a specific model of homogeneous-system free energy $g(\phi)$ in the functional (2.2).

Once the exact OP profile $\phi_0(z)$ of the planar interface has been determined for the given g, the explicit values of σ_m and δ_m, and of $\epsilon_m \equiv \epsilon^L(T_m)$ can be computed. While σ_m and ϵ_m are strictly positive quantities, the sign of δ_m is not *a priori* definite. A special but sufficiently general case of g function is the following:

$$g(\phi; T = T_m) = c_{20}\phi^2 \left(1 - \frac{\phi}{\phi_{s0}}\right)^2$$
$$\times \left[1 + (\gamma_5 + 2\gamma_6)\frac{\phi}{\phi_{s0}} + \gamma_6 \frac{\phi^2}{\phi_{s0}^2}\right] \quad (A1)$$

with $\gamma_5 > -1 - 3\gamma_6$ for $0 < \gamma_6 \le 1$ and $\gamma_5 > -2\gamma_6 - 2\sqrt{\gamma_6}$ for $\gamma_6 > 1$. Equation (A1) is the most general sixth-degree polynomial which admits two non-equivalent minimum valleys at 0 and ϕ_{s0}, and no further negative minimum between them. For this g, the differential equation (2.4) is still too difficult to solve in closed form for generic κ, even when $\gamma_5 = \gamma_6 = 0$. Hence, we decided to work perturbatively in κ, γ_5, and γ_6.

At zeroth order, i.e., $\kappa = \gamma_5 = \gamma_6 = 0$, corresponding to ϕ^4 theory, the solution to (2.4) is

$$\overline{\phi}_0(z) = \frac{\phi_{s0}}{2}\left\{1 - \tanh\left(\frac{z - C}{\ell}\right)\right\} \quad (A2)$$

with $\ell = \sqrt{2c/c_{20}}$ and arbitrary C. We fix C by requiring that the interface is centered at $z = 0$ (hence $C = 0$). Then, by still keeping $\gamma_5 = \gamma_6 = 0$, we switch on κ and search for a second-order solution to Eq. (2.4) in the form

$$\phi_0(z) = \overline{\phi}_0(z) + \frac{\kappa}{c\ell^2}\chi_1(z) + \left(\frac{\kappa}{c\ell^2}\right)^2 \chi_2(z). \quad (A3)$$

We thus arrive at the two equations:

$$c\overline{\phi}_0'\chi_1' - g_0'(\overline{\phi}_0)\chi_1 = c\ell^2\left(\overline{\phi}_0'\overline{\phi}_0''' - \frac{1}{2}\overline{\phi}_0''^2\right) \quad (A4)$$

and

$$c\overline{\phi}_0'\chi_2' - g_0'(\overline{\phi}_0)\chi_2 = c\ell^2(\overline{\phi}_0'\chi_1''' + \chi_1'\overline{\phi}_0''' - \overline{\phi}_0''\chi_1'')$$
$$- \frac{c}{2}\chi_1'^2 + \frac{g_0''(\overline{\phi}_0)}{2}\chi_1^2, \quad (A5)$$

where

$$g_0(\phi) = c_{20}\phi^2 \left(1 - \frac{\phi}{\phi_{s0}}\right)^2. \quad (A6)$$

By requiring that $\phi_0(z)$ is centered at $z = 0$ we obtain

$$\chi_1(z) = \frac{\phi_{s0}}{\cosh^2(z/\ell)}\left(2\tanh\frac{z}{\ell} - \frac{z}{\ell}\right) \quad (A7)$$

and

$$\chi_2(z) = \frac{\phi_{s0}}{\cosh^2(z/\ell)}\left(32\tanh^3\frac{z}{\ell} - 12\frac{z}{\ell}\tanh^2\frac{z}{\ell} - 8\tanh\frac{z}{\ell}\right.$$
$$\left. + 2\left(\frac{z}{\ell}\right)^2 \tanh\frac{z}{\ell} - 3\frac{z}{\ell}\right). \quad (A8)$$

Hence, we find $\delta_m = 0$ since the function $c\phi_0'^2(z) + 2\kappa\phi_0''^2(z)$ is even. Actually, the result $\delta_m = 0$ is valid at any order in κ when $\gamma_5 = \gamma_6 = 0$ (see below). Up to second order in κ, the values of σ_m and ϵ_m are given by

$$\sigma_m = \left[1 + \frac{2}{5}\frac{\kappa}{c\ell^2} - \frac{38}{35}\left(\frac{\kappa}{c\ell^2}\right)^2\right]\frac{c\phi_{s0}^2}{3\ell},$$
$$\epsilon_m = \left[\frac{\pi^2 - 6}{12} + \left(\frac{26}{5} - \frac{\pi^2}{3}\right)\frac{\kappa}{c\ell^2}\right.$$
$$\left. + \left(\frac{1566}{175} - \frac{4\pi^2}{3}\right)\left(\frac{\kappa}{c\ell^2}\right)^2\right]\ell^2. \quad (A9)$$

Next, we take κ, γ_5, and γ_6 all non-zero and of the same order of magnitude, and search for a first-order solution to (2.4) in the form

$$\phi_0(z) = \overline{\phi}_0(z) + \gamma_5\psi_1(z) + \gamma_6\xi_1(z) + \frac{\kappa}{c\ell^2}\chi_1(z). \quad (A10)$$

Upon inserting (A10) into Eq. (2.4), we obtain two independent equations for $\psi_1(z)$ and $\xi_1(z)$, namely

$$c\overline{\phi}_0'\psi_1' - g_0'(\overline{\phi}_0)\psi_1 = \frac{\overline{\phi}_0 g_0(\overline{\phi}_0)}{\phi_{s0}} \quad (A11)$$

and

$$c\overline{\phi}_0'\xi_1' - g_0'(\overline{\phi}_0)\xi_1 = \left(2\frac{\overline{\phi}_0}{\phi_{s0}} + \frac{\overline{\phi}_0^2}{\phi_{s0}^2}\right)g_0(\overline{\phi}_0), \quad (A12)$$

while $\chi_1(z)$ is still given by Eq. (A7). The solutions to Eqs. (A11) and (A12) such that each term of (A10) separately meets the requirement of being centered at zero are the following:

$$\psi_1(z) = -\frac{\phi_{s0}}{8\cosh^2(z/\ell)}\left(1 - \ln 2 + \frac{z}{\ell} - \ln\cosh\frac{z}{\ell}\right) \quad (A13)$$

and

$$\xi_1(z) = -\frac{\phi_{s0}}{8\cosh^2(z/\ell)}\left[3(1 - \ln 2) + 3\frac{z}{\ell}\right.$$
$$\left. - 3\ln\cosh\frac{z}{\ell} - \frac{1}{2}\tanh\frac{z}{\ell}\right]. \quad (A14)$$

Upon plugging the by now specified $\phi_0(z)$ in the integrals defining σ_m, δ_m, and ϵ_m, we eventually obtain the formulae

$$\sigma_m = \left(1 + \frac{1}{4}\gamma_5 + \frac{13}{20}\gamma_6 + \frac{2}{5}\frac{\kappa}{c\ell^2}\right)\frac{c\phi_{s0}^2}{3\ell},$$

$$\delta_m = \frac{5}{48}(\gamma_5 + 3\gamma_6)\ell, \quad \text{and}$$

$$\epsilon_m = \left[\frac{\pi^2 - 6}{12} - \frac{\pi^2 - 6}{48}\gamma_5 - \left(\frac{17\pi^2}{240} - \frac{1}{2}\right)\gamma_6 \right.$$
$$\left. + \left(\frac{26}{5} - \frac{\pi^2}{3}\right)\frac{\kappa}{c\ell^2}\right]\ell^2. \qquad (A15)$$

We thus see that δ_m is generically non-zero and may be of both signs.

In conclusion, we give a proof that δ_m vanishes identically for

$$g(\phi) = c_{20}\phi^2\left(1 - \frac{\phi}{\phi_{s0}}\right)^2, \qquad (A16)$$

whatever κ is (a different argument can be found in Ref. 13). Let $\phi(z)$ be a solution to Eq. (2.4) obeying the boundary conditions

$$\phi(-\infty) = \phi_{s0}, \quad \phi(+\infty) = 0,$$
$$\phi'(\pm\infty) = \phi''(\pm\infty) = \ldots = 0. \qquad (A17)$$

There is an infinite number of such solutions, differing from each other by a simple translation. Let us first prove that $\widetilde{\phi}(z) \equiv \phi_{s0} - \phi(-z)$ is also a solution to (2.4). We have

$$g(\widetilde{\phi}(z)) = g(\phi(-z)); \quad \widetilde{\phi}'(z) = \phi'(-z); \quad \widetilde{\phi}''(z) = -\phi''(-z);$$
$$\widetilde{\phi}'''(z) = \phi'''(-z). \qquad (A18)$$

We thus see that

$$\kappa\widetilde{\phi}'(z)\widetilde{\phi}'''(z) - \frac{c}{2}\widetilde{\phi}'^2(z) - \frac{\kappa}{2}\widetilde{\phi}''^2(z) + g(\widetilde{\phi}(z))$$
$$= \kappa\phi'(-z)\phi'''(-z) - \frac{c}{2}\phi'^2(-z) - \frac{\kappa}{2}\phi''^2(-z) + g(\phi(-z)) = 0,$$
$$(A19)$$

since Eq. (2.4) is satisfied by ϕ for any z. Hence, $\widetilde{\phi}(z)$ obeys the differential equation (2.4). Moreover, like $\phi(z)$, $\widetilde{\phi}(z)$ also satisfies the conditions (A17). This is not yet sufficient to conclude that $\widetilde{\phi}(z)$ and $\phi(z)$ are the same function since they could differ by a translation along z. However, if among the infinite possibilities the one is selected such that $\phi(0) = \phi_{s0}/2$, then $\widetilde{\phi}(0) = \phi_{s0}/2$ and the two functions coincide: $\widetilde{\phi}(z) = \phi(z)$, implying

$$\phi(z) + \phi(-z) = \phi_{s0} \quad \text{for any } z. \qquad (A20)$$

Upon differentiating (A20) with respect to z we find that $\phi'(-z) = \phi'(z)$ and the function $\phi'(z)$ is even. This is enough to conclude that $\int dz\, z\phi'(z) = 0$ (the interface is centered in 0). Differentiating (A20) once more, we obtain $\phi''(-z) = -\phi''(z)$ and $\phi''(z)$ is an odd function of z (while $\phi''^2(z)$ is even). As a result, $\sigma_m\delta_m = -\int dz\, z[c\phi'^2(z) + 2\kappa\phi''^2(z)] = 0$ and the proof is complete.

APPENDIX B: DERIVATION OF EQ. (3.4)

Let ℓ be a curve in Σ parametrized by the arc length s and denote $(\mathbf{t}, \mathbf{n}, \mathbf{b})$ the Frenet trihedron in $\mathbf{R}(u_0, v_0) \in \ell$. Note that we are using nearly the same symbol for the normal to Σ ($\hat{\mathbf{n}}$) and for the normal vector to ℓ in $\mathbf{R}(u_0, v_0)$ ($\mathbf{n}$), though the two vectors are generally distinct. Now consider the Darboux frame $(\mathbf{T}, \mathbf{N}, \mathbf{B})$ with $\mathbf{T} = \mathbf{t}$, $\mathbf{N} = \hat{\mathbf{n}}$ (the unit normal to Σ in $\mathbf{R}(u_0, v_0)$), and $\mathbf{B} = \mathbf{T} \wedge \mathbf{N}$. Clearly, by a convenient rotation around $\mathbf{T} = \mathbf{t}$, $\mathbf{n}$ and $\mathbf{b}$ are carried to $\mathbf{N}$ and $\mathbf{B}$, respectively. Calling $\alpha(s)$ the rotation angle,

$$\begin{pmatrix} \mathbf{T} \\ \mathbf{N} \\ \mathbf{B} \end{pmatrix} = \begin{pmatrix} 1 & 0 & 0 \\ 0 & \cos\alpha & \sin\alpha \\ 0 & -\sin\alpha & \cos\alpha \end{pmatrix} \begin{pmatrix} \mathbf{t} \\ \mathbf{n} \\ \mathbf{b} \end{pmatrix}. \qquad (B1)$$

Using the Frenet-Serret formulae, namely

$$\frac{d\mathbf{t}}{ds} = \kappa\mathbf{n},$$
$$\frac{d\mathbf{n}}{ds} = -\kappa\mathbf{t} + \tau\mathbf{b}, \qquad (B2)$$
$$\frac{d\mathbf{b}}{ds} = -\tau\mathbf{n},$$

where κ is the curvature and τ is the torsion of ℓ, we easily get

$$\begin{pmatrix} d\mathbf{T}/ds \\ d\mathbf{N}/ds \\ d\mathbf{B}/ds \end{pmatrix} = \begin{pmatrix} 0 & \kappa_n & \kappa_g \\ -\kappa_n & 0 & \tau_g \\ -\kappa_g & -\tau_g & 0 \end{pmatrix} \begin{pmatrix} \mathbf{T} \\ \mathbf{N} \\ \mathbf{B} \end{pmatrix}, \qquad (B3)$$

where $\kappa_n = \kappa\cos\alpha$ is the normal curvature, $\kappa_g = -\kappa\sin\alpha$ the geodetic curvature, and $\tau_g = \tau + d\alpha/ds$ the geodetic torsion.

For the u-lines, if we identify $\mathbf{T}$ with $\mathbf{R}_u$ then $\mathbf{B} = \mathbf{T} \wedge \mathbf{N} = -\mathbf{R}_v$. Similarly, for the v-lines, if we identify $\mathbf{T}$ with $\mathbf{R}_v$ then $\mathbf{B} = \mathbf{T} \wedge \mathbf{N} = \mathbf{R}_u$. We thus obtain

$$\frac{\partial\hat{\mathbf{n}}}{\partial u} = -\kappa_n^{(1)}\mathbf{R}_u - \tau_g^{(1)}\mathbf{R}_v \quad \text{and} \quad \frac{\partial\hat{\mathbf{n}}}{\partial v} = \tau_g^{(2)}\mathbf{R}_u - \kappa_n^{(2)}\mathbf{R}_v. \qquad (B4)$$

Moreover,

$$\frac{\partial\mathbf{R}_u}{\partial u} = -\kappa_g^{(1)}\mathbf{R}_v + \kappa_n^{(1)}\hat{\mathbf{n}} \quad \text{and} \quad \frac{\partial\mathbf{R}_u}{\partial v} = -\kappa_g^{(2)}\mathbf{R}_v - \tau_g^{(2)}\hat{\mathbf{n}},$$
$$\frac{\partial\mathbf{R}_v}{\partial u} = \kappa_g^{(1)}\mathbf{R}_u + \tau_g^{(1)}\hat{\mathbf{n}} \quad \text{and} \quad \frac{\partial\mathbf{R}_v}{\partial v} = \kappa_g^{(2)}\mathbf{R}_u + \kappa_n^{(2)}\hat{\mathbf{n}}. \qquad (B5)$$

From $\mathbf{R}_{uv} = \mathbf{R}_{vu}$, we derive

$$\kappa_g^{(1)}\mathbf{R}_u + \kappa_g^{(2)}\mathbf{R}_v + \left(\tau_g^{(1)} + \tau_g^{(2)}\right)\hat{\mathbf{n}} = 0. \qquad (B6)$$

Since $\mathbf{R}_u$, $\mathbf{R}_v$, and $\hat{\mathbf{n}}$ are linearly independent, it necessarily follows that

$$\kappa_g^{(1)} = \kappa_g^{(2)} = 0 \quad \text{and} \quad \tau_g^{(2)} = -\tau_g^{(1)} \equiv -\tau_g. \qquad (B7)$$

Since the geodetic curvature vanishes, our assumption that $\mathbf{R}_u$ and $\mathbf{R}_v$ are orthonormal vectors implies that the coordinate lines are surface geodesics.

Finally, putting Eqs. (B4) and (B7) together we promptly get Eq. (3.4).

APPENDIX C: SMALL FLUCTUATIONS ABOUT A SPHERICAL INTERFACE

We here provide the detailed derivation of Eq. (4.4) for the free energy of a quasispherical interface Σ. The starting point is the expansion of the relative amount of asphericity, $\epsilon(\theta, \phi)$, in real spherical harmonics, Eq. (4.3). In view of the smallness of the expansion coefficients $x_{l,m}$, the enclosed volume and area of Σ can be approximated as

$$
\mathcal{V}[\Sigma] = \frac{1}{3} \int_{\Sigma} dS \, \mathbf{r} \cdot \hat{\mathbf{n}}
$$
$$
= \frac{4}{3} \pi R_0^3 + R_0^3 \sum_{l>0,m} x_{l,m}^2 \equiv \frac{4}{3} \pi R_0^3 f(\{x\}) \quad \text{(C1)}
$$

and

$$
\mathcal{A}[\Sigma] = \int_{\Sigma} dS = 4\pi R_0^2 + \frac{R_0^2}{2} \sum_{l>0,m} (l^2 + l + 2) x_{l,m}^2
$$
$$
\equiv 4\pi R_0^2 \, g(\{x\}), \quad \text{(C2)}
$$

$f(\{x\})$ and $g(\{x\})$ being close-to-1 factors. In writing the two formulae above we supposed $x_{0,0} = 0$, which can always be assumed by suitably redefining in $R(\theta, \phi)$ the radius R_0 and the other coefficients $x_{l,m}$. In order to evaluate the mean curvature H, we start from

$$
\nabla \cdot \hat{\mathbf{n}} = \frac{1}{r^2} \frac{\partial(r^2 \hat{n}_r)}{\partial r} + \frac{1}{r \sin \theta} \frac{\partial}{\partial \theta} (\sin \theta \, \hat{n}_\theta) + \frac{1}{r \sin \theta} \frac{\partial \hat{n}_\phi}{\partial \phi},
$$
$$
\text{(C3)}
$$

where

$$
\hat{n}_r = 1 - \frac{1}{2} \epsilon_\theta^2 - \frac{1}{2} \frac{\epsilon_\phi^2}{\sin^2 \theta},
$$
$$
\hat{n}_\theta = -\epsilon_\theta (1 - \epsilon),
$$
$$
\hat{n}_\phi = -\frac{\epsilon_\phi (1 - \epsilon)}{\sin \theta}. \quad \text{(C4)}
$$

From that we get

$$
\nabla \cdot \hat{\mathbf{n}} = \frac{2}{R(\theta, \phi)} \left(1 + \frac{1}{2} L^2 \epsilon(\theta, \phi) - \frac{1}{2} \epsilon(\theta, \phi) L^2 \epsilon(\theta, \phi) \right),
$$
$$
\text{(C5)}
$$

where

$$
L^2 = -\frac{1}{\sin \theta} \frac{\partial}{\partial \theta} \left(\sin \theta \frac{\partial}{\partial \theta} \right) - \frac{1}{\sin^2 \theta} \frac{\partial^2}{\partial \phi^2}. \quad \text{(C6)}
$$

Eventually, we obtain

$$
\int_{\Sigma} dS (\sigma_m - 2\sigma_m \delta_m H + 2\lambda H^2)
$$
$$
= 4\pi \sigma_m R_0^2 + \frac{\sigma_m R_0^2}{2} \sum_{l>0,m} (l^2 + l + 2) x_{l,m}^2 - 8\pi \sigma_m \delta_m R_0
$$
$$
- \sigma_m \delta_m R_0 \sum_{l>0,m} l(l+1) x_{l,m}^2 + 8\pi \lambda + \frac{\lambda}{2}
$$
$$
\times \sum_{l>1,m} l(l+1)(l-1)(l+2) x_{l,m}^2. \quad \text{(C7)}
$$

Finally, we specify the integral measure in (4.2):

$$
\int \mathcal{D}\Sigma = \int_{-\infty}^{+\infty} \prod_{l>0,m} \left(\frac{S}{s} dx_{l,m} \right) \int_0^{+\infty} \frac{dR_0}{a}, \quad \text{(C8)}
$$

where $S = (36\pi)^{1/3} V^{2/3}$ is the area of the spherical surface of volume V and $s = 4\pi a^2$. Equation (C8) follows from requiring that the present theory (in fact the theory with an upper cutoff on l, see below) should coincide with the continuum limit of the field theory for a solid-on-solid (SOS) model with real heights defined on nodes uniformly placed over a sphere of radius $\sqrt{S/(4\pi)}$.

To prove this, first observe that the equation for the generic Σ entering in the functional integral is $R - R_0 = \sum_{l>0,m} R_0 Y_{l,m}(\theta, \phi) x_{l,m}$. Since $R_0 = \sqrt{S/(4\pi)}$ up to terms $\mathcal{O}(x_{l,m}^2)$, the height profile which the equation for Σ corresponds to is

$$
h_i = \sum_{l>0,m} \sqrt{\frac{S}{4\pi}} Y_{l,m}(\Omega_i) x_{l,m}, \quad \text{(C9)}
$$

for $i = 1, 2, \ldots, n$ and $n = (l_{\max} + 1)^2 - 1 \simeq S/a^2$ (the necessity of an upper cutoff $l_{\max}$ on l given by the following Eq. (C17) will be motivated later). The relation between the two theories passes through the identification

$$
\int \prod_{i=1}^n \frac{dh_i}{a} \quad \leftrightarrow \quad \int \frac{J}{a^n} \prod_{l>0,m} dx_{l,m}, \quad \text{(C10)}
$$

where J is the Jacobian of the transformation (C9):

$$
J \equiv \det \left(\frac{\partial h_i}{\partial x_{l,m}} \right) = \left(\frac{S}{4\pi} \right)^{n/2} \begin{vmatrix} Y_{1,-1}(\Omega_1) & \ldots & Y_{l_{\max},l_{\max}}(\Omega_1) \\ \vdots & \ddots & \vdots \\ Y_{1,-1}(\Omega_n) & \ldots & Y_{l_{\max},l_{\max}}(\Omega_n) \end{vmatrix}.
$$
$$
\text{(C11)}
$$

Called $\Delta\Omega = 4\pi/n$ the element of solid angle assigned to each node Ω_i, we have

$$
\sum_i Y_{l,m}(\Omega_i) Y_{l',m'}(\Omega_i) \approx \frac{1}{\Delta\Omega} \int d^2\Omega \, Y_{l,m}(\Omega) Y_{l',m'}(\Omega)
$$
$$
= \frac{1}{\Delta\Omega} \delta_{l,l'} \delta_{m,m'}. \quad \text{(C12)}
$$

Hence, for sufficiently large n the columns of the matrix (C11) are mutually orthogonal n-vectors. In order that every column vector be normalized, it suffices to multiply the whole matrix in (C11) by $\sqrt{\Delta\Omega}$, thus getting an orthogonal matrix (of unit determinant). Therefore, we find

$$
\frac{J}{a^n} = \left(\frac{S}{4\pi a^2} \right)^n, \quad \text{(C13)}
$$

which amounts to take $s = 4\pi a^2$ in Eq. (C8). This completes our proof.

We can now go on to compute the partition function (4.2). We first calculate the integral on R_0 by rearranging the delta function in Z_s as

$$
\delta \left(\frac{4}{3} \pi R_0^3 f(\{x\}) - V \right) = \frac{\delta(R_0 - [4\pi f(\{x\})/(3V)]^{-1/3})}{(36\pi)^{1/3} V^{2/3} f(\{x\})^{1/3}}.
$$
$$
\text{(C14)}
$$

After doing the trivial integral on R_0, we remain with a factor $f(\{x\})^{-1/3}$ which, within a quadratic theory, can be treated as follows:

$$
f(\{x\})^{-1/3} = \left(1 + \frac{3}{4\pi} \sum_{l>0,m} x_{l,m}^2\right)^{-1/3}
$$

$$
\simeq 1 - \frac{1}{4\pi} \sum_{l>0,m} x_{l,m}^2
$$

$$
\simeq \exp\left\{-\frac{1}{4\pi} \sum_{l>0,m} x_{l,m}^2\right\}. \tag{C15}
$$

In the end, we arrive at a Gaussian integral which is readily computed,

$$
Z_s = (36\pi)^{-1/3} \left(\frac{V}{a^3}\right)^{-2/3}
$$

$$
\times \exp\left\{\beta\rho_s|\Delta\mu|V - \beta\sigma_m S - 8\pi\beta\lambda\right.
$$

$$
\left. + 8\pi\beta\sigma_m\delta_m \left(\frac{3V}{4\pi}\right)^{1/3}\right\}
$$

$$
\times \left(\frac{2\pi S}{s}\right)^3 \prod_{l>1}\left\{\left(\frac{s}{2\pi S}\right)^2 \left[1 + \frac{\beta\sigma_m S}{2}(l^2 + l - 2)\right.\right.
$$

$$
+ 2\pi\beta\lambda\, l(l+1)(l-1)(l+2)
$$

$$
\left.\left. - 4\pi\beta\sigma_m\delta_m \sqrt{\frac{S}{4\pi}}(l^2 + l - 2)\right]\right\}^{-(l+1/2)}. \tag{C16}
$$

Without a proper ultraviolet cutoff $l_{\max}$ the l sum in $\ln Z_s$ does not converge. This is a typical occurrence for field theories on the continuum, which do not consider the granularity of matter at the most fundamental level. We fix $l_{\max}$ by requiring that the total number of (l,m) modes be equal to the average number of SOS heights/atoms on the cluster surface. It thus follows:

$$
l_{\max} = \frac{\sqrt{S}}{a} - 1. \tag{C17}
$$

With this cutoff, the surface free energy becomes $F_s = \sigma(S)S$, with an interface tension $\sigma(S)$ dressed by thermal fluctuations,

$$
\sigma(S) = \sigma_m + \frac{k_B T}{2S} \sum_{l=2}^{\sqrt{S}/a-1} (2l+1)
$$

$$
\times \ln[A + B(l^2 + l - 2) + C(l^2 + l - 2)^2]
$$

$$
- 2\sigma_m\delta_m \left(\frac{4\pi}{S}\right)^{1/2} - 2\frac{k_B T}{S} \ln\left(\frac{S}{a^2}\right)
$$

$$
- 3\frac{k_B T}{S} \ln\left(\frac{2\pi a^2}{s}\right) + \frac{8\pi\lambda}{S}. \tag{C18}
$$

The quantities A, B, and C in Eq. (C18) are given by

$$
A = \frac{A_0}{S^2}, \quad B = \frac{2C_0}{S^2} + \frac{D_0}{S\sqrt{S}} + \frac{B_0}{S}, \quad C = \frac{C_0}{S^2}, \tag{C19}
$$

where

$$
A_0 = \frac{s^2}{4\pi^2}, \quad B_0 = \frac{\beta\sigma_m s^2}{8\pi^2}, \quad C_0 = \frac{\beta\lambda s^2}{2\pi},
$$

$$
D_0 = -\frac{\beta\sigma_m\delta_m s^2}{2\pi\sqrt{\pi}}. \tag{C20}
$$

By the Euler-Mac Laurin formula, the residual sum in Eq. (C18) can be evaluated explicitly. After a tedious and rather lengthy derivation, we obtain (for $\lambda \neq 0$):

$$
\sigma(S) = \sigma_m + \frac{k_B T}{2a^2}\left[\ln\frac{B_0}{a^2 e^2} + \left(1 + \frac{B_0 a^2}{C_0}\right)\ln\left(1 + \frac{C_0}{B_0 a^2}\right)\right]
$$

$$
+ \left[-2\sigma_m\delta_m + \frac{k_B T D_0}{4C_0\sqrt{\pi}}\ln\left(1 + \frac{C_0}{B_0 a^2}\right)\right]\left(\frac{4\pi}{S}\right)^{1/2}
$$

$$
- \frac{7}{6}k_B T \frac{\ln(S/a^2)}{S} + \left[8\pi\beta\lambda - 3\ln\frac{2\pi a^2}{s} - \frac{11}{6}\ln\frac{B_0}{a^2}\right.
$$

$$
+ 3 - \frac{5}{3}\ln 2 - \frac{25}{96} + \frac{121}{46080} + \frac{D_0 a}{4C_0} - \frac{D_0^2}{4B_0 C_0}
$$

$$
- \frac{1}{6}\ln\left(\frac{B_0}{a^2} + \frac{C_0}{a^4}\right) + \frac{1}{8C_0(B_0 a^2 + C_0)^2}
$$

$$
\times \left(-4B_0 C_0 D_0 a^3 - 18 B_0 C_0^2 a^2 - 2C_0^2 D_0 a - \frac{28}{3}C_0^3\right.
$$

$$
- \frac{26}{3}B_0^2 C_0 a^4 - 2B_0^2 D_0 a^5 + 2B_0 D_0^2 a^4
$$

$$
\left.\left. + 2C_0 D_0^2 a^2\right)\right]\frac{k_B T}{S}, \tag{C21}
$$

up to terms $o(S^{-1})$. We wrote a computer code to evaluate the sum in (C18) numerically for large S, and so checked that every single term in Eq. (C21) is indeed correct.

APPENDIX D: ANISOTROPIC-INTERFACE MODELS OF NUCLEATION

We here show that nonperturbative corrections to CNT do also arise when the interface tension is infinitely anisotropic. In this case, the admissible cluster shapes are all regular and the functional integral (4.2) is greatly simplified, reducing to a standard integral over the few independent variables which concur to define the allowed clusters. The terms in (3.15) beyond the surface-tension term do also contribute to the total surface free energy if anisotropy is strong but not infinitely so.

Our argument goes as follows. Let us, for instance, consider the interface tension (4.5). For $M \gg 1$, we expect that the leading contribution to the functional integral (4.2) be given by rectangular cuboids with slightly rounded edges and vertices. Since we are only interested in making a rough estimation of the relative magnitude of each contribution to H_s, we assume that the surface of a rounded edge is one fourth of a cylindrical surface ($H = 1/a$) whereas that of a rounded vertex is an octant of a sphere ($H = 2/a$), a being a microscopic diameter. Also observe that: $\sigma_{100} \sim k_B T_m/a^2$; the average value of $\sigma(\hat{n})$ on an edge or vertex is $\sim M\sigma_{100}$; the Tolman length is $\delta_m \sim a$; and λ is roughly κ/c times σ_m, hence $\lambda \sim \sigma_m a^2$. We now decompose (3.15) into the sum of three integrals,
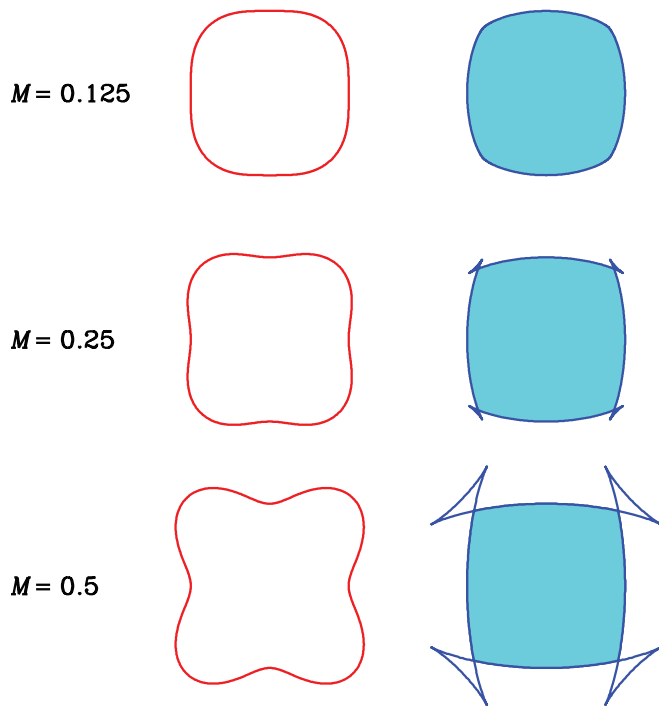
FIG. 3. Two-dimensional Wulff construction for a square cluster. Left: Polar plot of the interface tension σ in Eq. (D1) (red curves) as a function of the normal $\hat{\mathbf{n}} = \cos\phi\,\hat{\mathbf{x}} + \sin\phi\,\hat{\mathbf{y}}$ to a cluster face, for three distinct values of M. Right: Equilibrium cluster shape as the envelope of the family of perpendicular planes (blue curves). In this case, the cluster of minimum surface energy (colored in cyan) has curved faces, but sharp corners. The envelope continues beyond the corners, but these parts have no physical meaning.

respectively, over faces, edges, and vertices. Denoting l_1, l_2, l_3 (all much larger than a) the side lengths of the cuboid if its edges and vertices were taken to be sharp, the integral over faces is practically equal to $2\sigma_{100}(l_1 l_2 + l_1 l_3 + l_2 l_3) \sim k_B T_m (l_1 l_2 + l_1 l_3 + l_2 l_3)/a^2$; up to a factor of order one, the integral over edges is given by $M k_B T_m (l_1 + l_2 + l_3)/a$; finally, the integral over vertices is of the order of $M k_B T_m$. We then see that, when $M \to \infty$ for fixed a, only faces contribute to the integral (4.2), while edges and vertices would only matter if M were finite.

In general terms, from the knowledge of the "Wulff plot" $\sigma(\hat{\mathbf{n}})$, the equilibrium cluster shape follows from the so-called Wulff construction:[44] (i) draw the planes perpendicular to the unit vectors $\hat{\mathbf{n}}$ and at a distance $\sigma(\hat{\mathbf{n}})$ away from the origin; (ii) for each plane, discard the half-space of $\mathbb{R}^3$ that lies on the far side of the plane from the origin. The convex region consisting of the intersection of the retained half-spaces is the cluster of lowest surface energy. When $\sigma(\hat{\mathbf{n}})$ is smooth, this Wulff cluster is bounded by part of the envelope of the planes; the parts of the envelope not bounding the convex body – the "ears" or "swallowtails" which are, e.g., visible in Figs. 3 and 6 below – are unphysical.

1. Rectangles

In two dimensions, a rudimentary model of nucleation is that which only allows for rectangular clusters. This is relevant for two-dimensional crystals of square symmetry, and could be obtained from a smooth interface tension of

the form

$$\sigma(\phi) = \sigma_{10}[1 + M \sin^2(2\phi)] \tag{D1}$$

upon taking the infinite-M limit. In Eq. (D1), ϕ is the polar angle of the normal vector while σ_{10} is the free energy of the cheapest, (10) facet. As $M \to \infty$, all normal directions different from [10], [01], [$\bar{1}$0], and [0$\bar{1}$] are excluded from the equilibrium cluster shape and a perfectly square surface is obtained. This is illustrated in Fig. 3 for three values of M; here and elsewhere, the envelope of perpendicular planes is given, in parametric terms, by the equations:[45]

$$x = \cos\phi\,\sigma(\phi) - \sin\phi\,\sigma'(\phi),$$
$$y = \sin\phi\,\sigma(\phi) + \cos\phi\,\sigma'(\phi). \tag{D2}$$

Note that the edge fluctuations deforming the square in a rectangle are still allowed by (D1) in the infinite-M limit, since rectangles and cubes share the same type of facets. Hence, assuming that only rectangular shapes have a non-zero Boltzmann weight in the functional integral (4.2), the surface free energy reduces to:

$$F_s(V) = -\frac{1}{\beta} \ln \int_0^{+\infty} da \int_0^{+\infty} db\, e^{-2\beta\sigma(a+b)} \delta(ab - V) \tag{D3}$$

We easily find:

$$\beta \Delta G(V)$$
$$\equiv -\beta g V + \beta F_s(V)$$
$$= -\beta g V + 4\beta\sigma\sqrt{V} - \ln \int_{-\infty}^{+\infty} dx\, \exp\{-\tau(\cosh x - 1)\}$$
$$= -\beta g V + 4\beta\sigma\sqrt{V} - \ln \left\{ 2e^\tau \int_1^{+\infty} dt\, \frac{e^{-\tau t}}{\sqrt{t^2 - 1}} \right\}$$
$$= -\beta g V + 4\beta\sigma\sqrt{V} - \ln \left\{ 2e^\tau K_0(\tau) \right\}, \tag{D4}$$

where g is proportional to the supersaturation, $\tau = 4\beta\sigma\sqrt{V}$, and K_0 is a modified Bessel function of the second kind. The last term in Eq. (D4) is the full correction to CNT as formulated for squares. A typical profile of $\beta\Delta G(V)$ is plotted in Fig. 4.

At variance with CNT, $\Delta G(V)$ shows a weak divergence to $-\infty$ for $V \to 0$, due to the absence of a lower cutoff volume. For $\tau \ll 1$,

$$K_0(\tau) = -\ln(\tau/2) - \gamma + \mathcal{O}(\tau^2 \ln\tau), \tag{D5}$$

with $\gamma = 0.5772\ldots$ (Eulero-Mascheroni constant). Hence, the singular behavior of $\beta\Delta G(V)$ for small V is of the kind

$$\beta\Delta G(V) \simeq -\ln\{-\ln(2\beta\sigma\sqrt{V})\}. \tag{D6}$$

Conversely, for large τ values,

$$K_0(\tau) \sim \sqrt{\frac{\pi}{2\tau}}\, e^{-\tau}, \tag{D7}$$

and we obtain

$$\beta\Delta G(V) \simeq -\beta g V + 4\beta\sigma\sqrt{V}$$
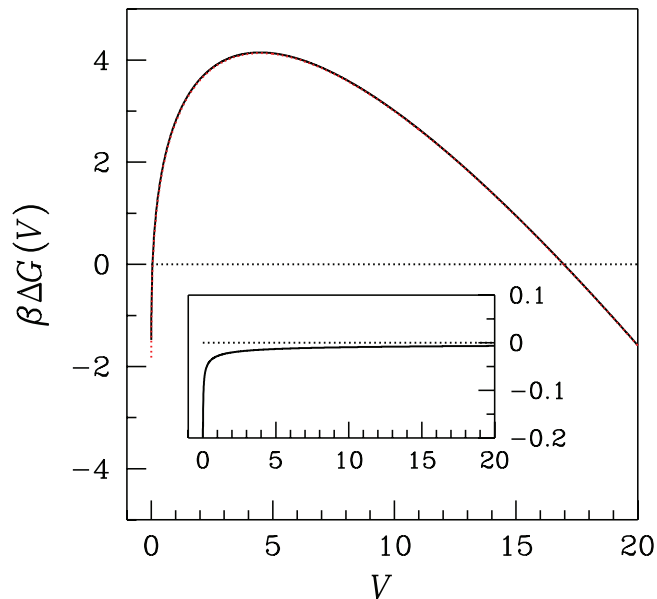$$+ \frac{1}{2}\ln(4\beta\sigma\sqrt{V}) - \frac{1}{2}\ln(2\pi). \tag{D8}$$

FIG. 4. Rectangles: $\beta\Delta G(V)$ vs. V for $\beta g = \beta\sigma = 1$ (black solid line). The dotted red line corresponds to the approximant (D8). Inset: The difference between (D8) and $\beta\Delta G(V)$.

The goodness of the approximation (D8) can be judged from the inset of Fig. 4, which shows that the approximation is accurate for all values of V but for the smallest ones.

2. Truncated rectangles

In order to study the effects on nucleation of a more complicate type of interface-tension anisotropy, we further enrich our book of patterns, passing from rectangles to truncated rectangles. By the name of truncated rectangle we mean the octagon represented in Fig. 5. This occurs when the cost of (11) and equivalent facets is of the same order of σ_{10}, while all other facets are much higher in energy and can be ruled out.
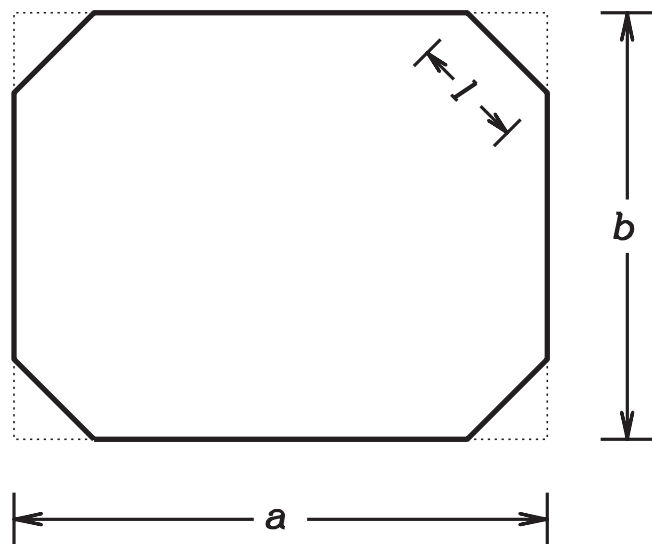

FIG. 5. A truncated rectangle. For fixed a and b, the maximum ℓ value is $\ell_{max} = (1/\sqrt{2})\min\{a, b\}$.
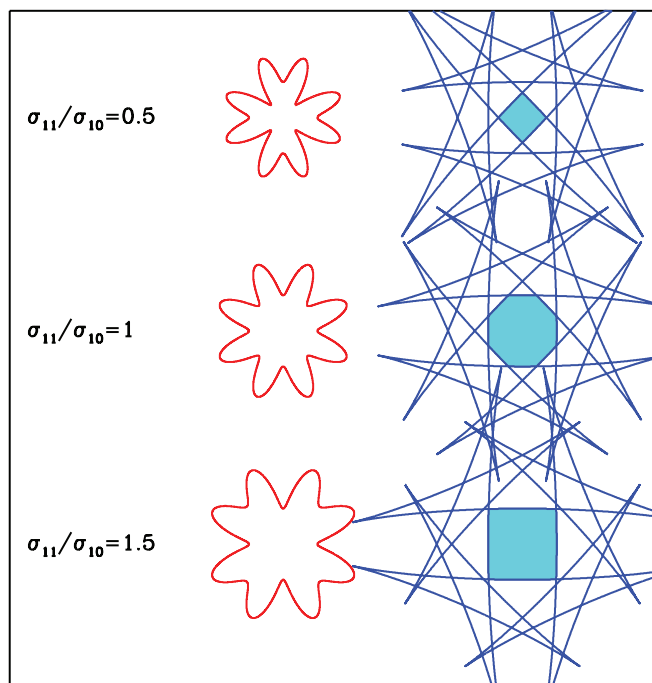

FIG. 6. Two-dimensional Wulff construction for the σ model at Eq. (D9), with $M = 1$. Left: Wulff plot (red) for three values of σ_{11}/σ_{10}. Right: Equilibrium cluster shape (the boundary of the cyan-colored region). The parts of the envelope of the family of perpendicular planes beyond the corners of the cluster are unphysical.

A Wulff plot giving origin to truncated squares is:

$$\sigma(\phi) = \sigma_{10}\left[1 + \left(\frac{\sigma_{11}}{\sigma_{10}} - 1\right)\sin^2(2\phi) + M\sin^2(4\phi)\right]$$

(D9)

with infinite M (see Fig. 6). The polar plot of (D9) for finite M is a smoothed eight-pointed star with hollows at the normal directions satisfying $\sin(4\phi) = 0$. Depending on the ratio of σ_{11} to σ_{10}, the equilibrium cluster shape shows (i) just (11) facets ($\sigma_{11}/\sigma_{10} \leq \sqrt{2}/2$); (ii) both (11) and (10) facets ($\sqrt{2}/2 < \sigma_{11}/\sigma_{10} < \sqrt{2}$); (iii) just (10) facets ($\sigma_{11}/\sigma_{10} \geq \sqrt{2}$).

In order to prove this, we observe that, for fixed a, b, and ℓ (with $\ell \leq \ell_{max} \equiv (1/\sqrt{2})\min\{a, b\}$), the "volume" and "area" of the truncated rectangle are given, respectively, by $V = ab - \ell^2$ and $A = A_{11} + A_{10}$, with $A_{11} = 4\ell$ and $A_{10} = 2(a + b - 2\sqrt{2}\ell)$, leading to a surface energy of

$$E_s = 4\sigma_{11}\ell + 2\sigma_{10}(a + b - 2\sqrt{2}\ell).$$

(D10)

To determine the cluster shape at zero temperature, E_s should be minimized as a function of a, b, and ℓ under the constraint of a fixed $ab - \ell^2 (= V)$. Setting $a = x\sqrt{V}$ and $b = y\sqrt{V}$ (with $x, y > 0$), we are led to minimize $4(\sigma_{11} - \sqrt{2}\sigma_{10})\sqrt{xy - 1} + 2\sigma_{10}(x + y)$ as a function of x and y. By

a straightforward calculation we find:

$$x = y = 1 \quad (\ell = 0), \quad \text{for } \frac{\sigma_{11}}{\sigma_{10}} \geq \sqrt{2};$$

$$x = y = \frac{1}{\sqrt{1 - (\sqrt{2} - \sigma_{11}/\sigma_{10})^2}}$$

$$\left(\frac{\ell}{\sqrt{V}} = \frac{\sqrt{2} - \sigma_{11}/\sigma_{10}}{\sqrt{1 - (\sqrt{2} - \sigma_{11}/\sigma_{10})^2}} \right), \quad \text{for } \frac{\sqrt{2}}{2} < \frac{\sigma_{11}}{\sigma_{10}} < \sqrt{2};$$

$$x = y = \sqrt{2} \quad \left(\frac{\ell}{\sqrt{V}} = 1 \right), \quad \text{for } \frac{\sigma_{11}}{\sigma_{10}} \leq \frac{\sqrt{2}}{2}. \tag{D11}$$

The equilibrium cluster shape is then a square (respectively, a 45-degree tilted square) for σ_{11}/σ_{10} values larger than $\sqrt{2}$ (smaller than $\sqrt{2}/2$), while being a truncated square otherwise (see Fig. 6).

Now going to the nucleation model for truncated rectangles, the surface free energy reads:

$$F_s(V) = -\frac{1}{\beta} \ln \iint_0^{+\infty} \mathrm{d}a \, \mathrm{d}b$$

$$\times \int_0^{\ell_{\max}} \frac{\mathrm{d}\ell}{\ell_0} e^{-4\beta\sigma_{11}\ell} e^{-2\beta\sigma_{10}(a+b-2\sqrt{2}\ell)} \delta(ab - \ell^2 - V), \tag{D12}$$

where ℓ_0 is an arbitrary length. By integrating the delta out, we obtain:

$$\beta \Delta G(V)$$

$$= -\beta g V + 4\beta\sigma_{10}\sqrt{V} - \frac{1}{2} \ln \left(\frac{V}{\ell_0^2} \right)$$

$$- \ln \int_{-\infty}^{+\infty} \mathrm{d}x \int_0^{+\infty} \mathrm{d}y \, \Theta(\min\{e^x, (1+y^2)e^{-x}\} - \sqrt{2}y)$$

$$\times \exp\{-(\tau_{11} - \sqrt{2}\tau_{10})y\}$$

$$\times \exp\left\{ -\frac{\tau_{10}}{2}(e^x + (1+y^2)e^{-x} - 2) \right\}, \tag{D13}$$

where Θ is Heaviside's function, $\tau_{10} = 4\beta\sigma_{10}\sqrt{V}$, and $\tau_{11} = 4\beta\sigma_{11}\sqrt{V}$. For $\beta\sigma_{10} = 1$, $\ell_0 = 1$, and $\sigma_{11}/\sigma_{10} = 0.5$, 1, 2, 20, 200, the plot of (D13) is reported in Fig. 7. Note that a precritical minimum shows up for any finite value of σ_{11}/σ_{10}, which moves toward zero upon increasing the interface-tension anisotropy. An even more complex behavior is seen for $\sigma_{11}/\sigma_{10} = 0.5$, where a bump emerges beyond the critical maximum.

When $\sigma_{11} \gg \sigma_{10}$, it is natural to expect that the model of truncated rectangles reduces to the rectangular-cluster model. This can be proved analytically starting from Eq. (D12). First, a, b, and ℓ are rescaled by dividing by $\sqrt{V}$; then one observes that

$$\sqrt{V} e^{-4\beta\sigma_{11}\sqrt{V}\ell} \approx \frac{1}{2\beta\sigma_{11}} \delta(\ell). \tag{D14}$$

Hence, aside from a constant equal to $\ln(4\beta\sigma_{11})$, the $\beta\Delta G(V)$ function for truncated rectangles merges, for very large σ_{11}/σ_{10}, into the analogous function for rectangles. This fact is shown numerically in the inset of Fig. 7.
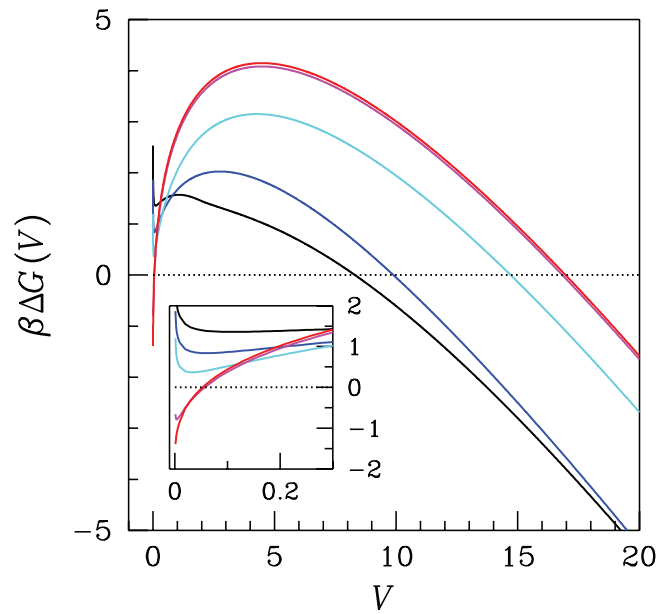

FIG. 7. Truncated rectangles: $\beta\Delta G(V)$ vs. V for $\beta g = \beta\sigma_{10} = 1$ e $\ell_0 = 1$. A constant of $\ln(4\beta\sigma_{11})$ was subtracted from $\beta\Delta G(V)$ in order to guarantee the confluence of its plot to that for rectangles, in the limit $\sigma_{11}/\sigma_{10} \to +\infty$. A number of σ_{11}/σ_{10} values are considered: 0.5 (black), 1 (blue), 2 (cyan), 20 (magenta), and 200 (red, practically indistinguishable from the rectangular case). In the inset, we zoom on the small-V region, evidencing the singular behavior of $\Delta G(V)$ for $V \to 0$. Apparently, for all finite σ_{11} values, the curve blows up to $+\infty$ rather than to $-\infty$, as instead occurs for rectangles.

3. Rectangular cuboids

When the Wulff plot is as in Eq. (4.5) with infinite M, the only admissible shapes are rectangular cuboids. Denoting a, b, and c the edges of a cuboid, the V-dependent surface free energy is defined as

$$\beta F_s(V) = -\ln \iiint_0^{+\infty} \mathrm{d}a \, \mathrm{d}b \, \mathrm{d}c \, e^{-2\beta\sigma(ab+ac+bc)} \delta(abc - V)$$

$$= -\ln \iint_0^{+\infty} \mathrm{d}a \, \mathrm{d}b \, \frac{1}{ab} \exp\left\{ -\frac{\tau}{3} \left(ab + \frac{a+b}{ab} \right) \right\}, \tag{D15}$$

where $\tau = 6\beta\sigma V^{2/3}$. With another change of variables, we arrive at

$$\beta\Delta G(V) = -\beta g V + 6\beta\sigma V^{2/3} - \ln \iint_{-\infty}^{+\infty} \mathrm{d}x \, \mathrm{d}y$$

$$\times \exp\left\{ -\frac{\tau}{3}(e^{x+y} + e^{-x} + e^{-y} - 3) \right\}. \tag{D16}$$

The above formula is well suited for the numerical evaluation of $\Delta G(V)$. For $\beta g = \beta\sigma = 1$, the profile of $\beta\Delta G(V)$ is plotted in Fig. 8.

In order to discover the analytic behavior of $\Delta G(V)$ at small and at large V's, we should further elaborate on Eq. (D16). Setting $a + b = x$ and $ab = y$ in (D15), a and b are the solutions to the equation $t^2 - xt + y = 0$, whose discriminant is non-negative for $x \geq 2\sqrt{y}$. Moreover, the Jacobian of the transformation is $1/\sqrt{x^2 - 4y}$. Hence, we get
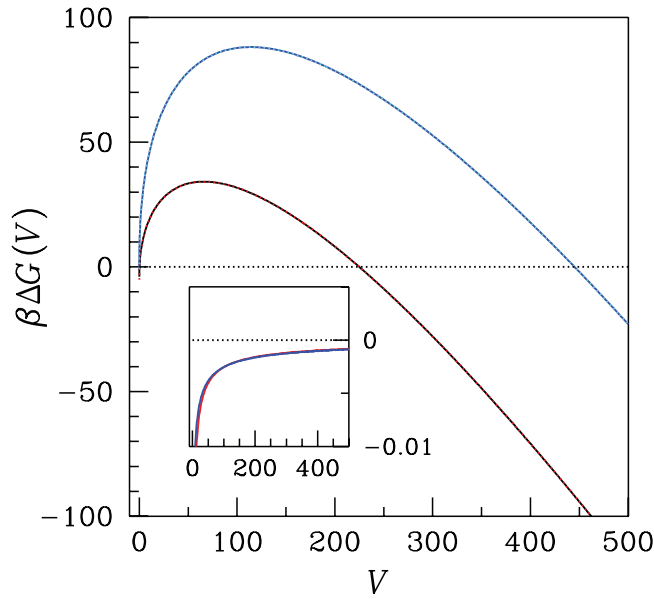
FIG. 8. Rectangular cuboids: $\beta\Delta G(V)$ vs. V for $\beta g = \beta\sigma = 1$ (black solid line). In blue, the same function when we include the cost of the edges ($\beta g = \beta\sigma = \beta\nu = 1$). The red dotted line is the approximant (D27) while the cyan dotted line is the approximant (D31). In the inset, we plot in red the difference between the approximation (D16) and (D27), and in blue the difference between (D28) and (D31).

$\beta F_s(V) \equiv -\ln I(V)$ with

$$I = 2\int_0^{+\infty} dy \int_{2\sqrt{y}}^{+\infty} dx \, \frac{\exp\{-(\tau/3)(y + x/y)\}}{y\sqrt{x^2 - 4y}}. \quad \text{(D17)}$$

With the further transformations $x \to z = \sqrt{x^2 - 4y}$ and $z \to w = z/y$, we eventually obtain:

$$I = 2\int_0^{+\infty} dy \, \frac{e^{-(\tau/3)y}}{y} \int_0^{+\infty} dz \, \frac{\exp\{-(\tau/3)\sqrt{z^2 + 4y}/y\}}{\sqrt{z^2 + 4y}}$$

$$= 2\int_0^{+\infty} dy \, \frac{e^{-(\tau/3)y}}{y} \int_0^{+\infty} dw \, \frac{\exp\left\{-\sqrt{w^2 + \frac{4\tau^2}{9y}}\right\}}{\sqrt{w^2 + \frac{4\tau^2}{9y}}}. \quad \text{(D18)}$$

Since

$$\int_0^{+\infty} dx \, \frac{\exp\{-\sqrt{x^2 + c^2}\}}{\sqrt{x^2 + c^2}} = \int_c^{+\infty} dt \, \frac{e^{-t}}{\sqrt{t^2 - c^2}} = K_0(c), \quad \text{(D19)}$$

we finally find:

$$I = 2\int_0^{+\infty} dy \, \frac{e^{-(\tau/3)y}}{y} K_0\left(\frac{2\tau}{3\sqrt{y}}\right)$$

$$= 4\int_0^{+\infty} dx \, \exp\left\{-\frac{4\tau^3}{27x^2}\right\} \frac{K_0(x)}{x}. \quad \text{(D20)}$$

In Eq. (D20) we recognize a particular Meijer function, $G_{03}^{30}((\tau/3)^3|0,0,0)$, whose behavior at small τ is

$$\frac{9}{2}(\ln\tau)^2 + 9(\gamma - \ln 3)\ln\tau + \mathcal{O}(1). \quad \text{(D21)}$$

From the above, we can draw the main singular term in $\beta\Delta G(V)$ at small V, that is

$$\beta\Delta G(V) \simeq -2\ln(-\ln(6\beta\sigma V^{2/3})), \quad \text{(D22)}$$

which is similar to (D6).

The large-V behavior of $\Delta G(V)$ can also be obtained from Eq. (D20). For $\tau \gg 1$, we are allowed to replace $K_0(x)$ with Eq. (D7) and thus estimate I through the integral

$$I_\infty = 2\sqrt{2\pi} \int_0^{+\infty} dx \, \frac{\exp\left\{-x - \frac{4\tau^3}{27x^2}\right\}}{x^{3/2}}. \quad \text{(D23)}$$

Suspecting a dominant term of τ in $-\ln I_\infty$, we consider

$$e^\tau I_\infty = 2\sqrt{\frac{2\pi}{\tau}} \int_0^{+\infty} dz \, z^{-3/2} \exp\left\{\tau\left(1 - z - \frac{4}{27z^2}\right)\right\}. \quad \text{(D24)}$$

In order to compute the asymptotic behavior of (D24), we use the Laplace method. The maximum of the concave function $\phi(z) = 1 - z - (4/27)z^{-2}$ falls at $c = 2/3$, with $\phi(c) = 0$ and $\phi''(c) = -9/2$. Since, for any $a < c < b$,

$$\int_a^b dz \, f(z) e^{\tau\phi(z)} \sim \frac{\sqrt{2\pi} f(c) e^{\tau\phi(c)}}{\sqrt{-\tau\phi''(c)}}, \quad \text{(D25)}$$

the asymptotic behavior of I reads

$$I \sim 2\pi\sqrt{3} \, \frac{e^{-\tau}}{\tau} \quad \text{(D26)}$$

and

$$\beta\Delta G(V) \sim -\beta g V + 6\beta\sigma V^{2/3} + \ln(6\beta\sigma V^{2/3}) - \ln(2\pi\sqrt{3}). \quad \text{(D27)}$$

The last two terms in Eq. (D27) give the subleading corrections to CNT as formulated for cubic clusters. The quality of the approximation (D27) can be judged from the inset of Fig. 8, which shows a very good matching for all V's except for the smallest values, similarly to what occurs for rectangles (cf. Fig. 4).

The calculation of ΔG can also be performed when a further energy cost, ν per unit length, is assumed for the edges. Equation (D16) is then modified to

$$\beta\Delta G(V) = -\beta g V + 6\beta\sigma V^{2/3} + 12\beta\nu V^{1/3}$$
$$- \ln \iint_{-\infty}^{+\infty} dx \, dy \, \exp\left\{-\frac{\tau_1}{3}(e^{x+y} + e^{-x}\right.$$
$$\left. + e^{-y} - 3) - \frac{\tau_2}{3}(e^{-x-y} + e^x + e^y - 3)\right\}, \quad \text{(D28)}$$

where $\tau_1 = 6\beta\sigma V^{2/3}$ and $\tau_2 = 12\beta\nu V^{1/3}$. By the same line of reasoning as followed above we arrive at $\beta F_s \equiv -\ln I(V)$ with

$$I = 2\int_0^{+\infty} dy \, \frac{e^{-(\tau_1/3)y - \tau_2/(3y)}}{y} K_0\left(\frac{2\tau_1}{3\sqrt{y}} + \frac{2\tau_2}{3}y\right). \quad \text{(D29)}$$

Laplace method can still be invoked to extract the asymptotic behavior of I, which turns out to be

$$-\ln I \sim \tau_1 + \tau_2 + \ln(\tau_1 + \tau_2) - \ln(2\pi\sqrt{3}). \quad \text{(D30)}$$

From the above formula, we get

$$\beta \Delta G(V) \sim -\beta g V + 6\beta\sigma V^{2/3} + 12\beta\nu V^{1/3}$$
$$+ \ln(6\beta\sigma V^{2/3} + 12\beta\nu V^{1/3}) - \ln(2\pi\sqrt{3}). \quad \text{(D31)}$$

In Fig. 8, we compare the approximation (D31) with the exact value. We see that the agreement is good for not too small V.

4. Ellipsoids

Let us finally study the case of an ellipsoidal cluster. Volume and area of an ellipsoid with semiaxes a, b, and c are, respectively, given by

$$V = \frac{4}{3}\pi abc \quad \text{and}$$

$$A = 2\pi\left(c^2 + \frac{bc^2}{\sqrt{a^2 - c^2}}F(\phi|m) + b\sqrt{a^2 - c^2}\,E(\phi|m)\right),$$

$$(a \geq b > c \text{ and } a > b \geq c\,;\; A = 4\pi c^2 \text{ for } a = b = c) \quad \text{(D32)}$$

where

$$m = \frac{a^2(b^2 - c^2)}{b^2(a^2 - c^2)} = \frac{1 - c^2/b^2}{1 - c^2/a^2} < 1$$

$$\text{and } \phi = \arcsin\frac{\sqrt{a^2 - c^2}}{a}. \quad \text{(D33)}$$

F and E are elliptic integrals of the first and second kind, respectively. For $-\pi/2 < \phi < \pi/2$, they are defined as

$$F(\phi|m) \equiv \int_0^\phi dx \frac{1}{\sqrt{1 - m\sin^2 x}}$$

$$\text{and } E(\phi|m) \equiv \int_0^\phi dx \sqrt{1 - m\sin^2 x}. \quad \text{(D34)}$$

Let now $A(a, b, c)$ be the surface area of an ellipsoid of semiaxes a, b, and c (not necessarily in descending order). By the usual transformations, the surface free energy becomes

$$\beta F_s(V) = -\ln\iint_0^{+\infty} da\,db\,\frac{1}{ab}$$

$$\times \exp\left\{-\beta\sigma\left(\frac{3V}{4\pi}\right)^{2/3} A\left(a, b, \frac{1}{ab}\right)\right\} + \ln\frac{4\pi}{3}$$

$$= \tau - \ln\iint_{-\infty}^{+\infty} dq\,dp$$

$$\times \exp\left\{-\frac{\tau}{4\pi}(A(e^q, e^p, e^{-q-p}) - 4\pi)\right\} + \ln\frac{4\pi}{3}, \quad \text{(D35)}$$

where $\tau = \beta\sigma(36\pi)^{1/3}V^{2/3}$. To obtain $\beta\Delta G(V)$, it is sufficient to add $-\beta g V$ to (D35). For $\beta g = \beta\sigma = 1$, the plot of
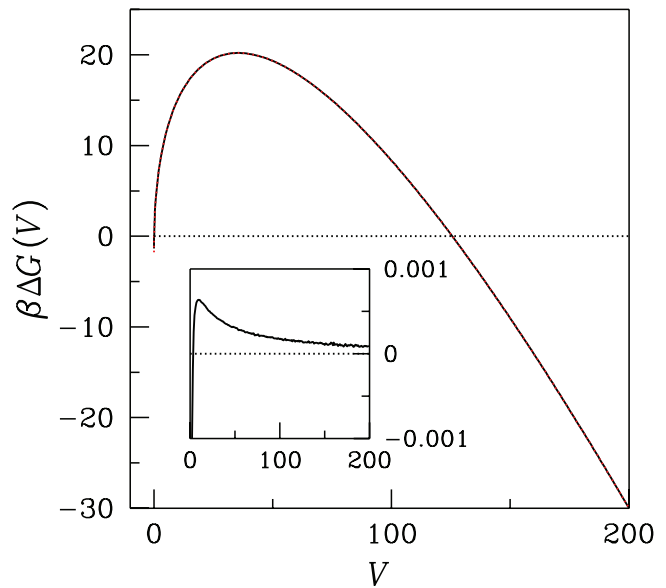

FIG. 9. Ellipsoids: $\beta\Delta G(V)$ vs. V for $\beta g = \beta\sigma = 1$ (black solid line). The red dotted line is the approximant (D36). Inset: The difference between the large-V estimate (D36) and the exact $\beta\Delta G(V)$.

this function is reported in Fig. 9. In the same figure, $\beta\Delta G(V)$ is compared with the asymptotic estimate

$$\beta\Delta G(V) \sim -\beta g V + \beta\sigma(36\pi)^{1/3}V^{2/3}$$
$$+ \ln(\beta\sigma(36\pi)^{1/3}V^{2/3}) - 0.4849, \quad \text{(D36)}$$

where the last two terms give the correction to CNT as formulated now for spherical clusters. Judging from the inset of Fig. 9, which shows the difference between the approximate and exact values of $\beta\Delta G(V)$, the estimate (D36) is very good for all V's except for the very small ones.

The strong similarity between (D27) and (D36), together with the high accuracy with which they reproduce the profile of $\beta\Delta G(V)$ for ellipsoids and cuboids, respectively, indicates that the difference between envisaging the nucleus as ellipsoidal rather than cuboidal entirely lies in the value of σ, which for an ellipsoid is $6/(36\pi)^{1/3} \simeq 1.241$ times the cuboidal one. This occurs exactly as in CNT where the same relation holds between the values of σ for spheres and cubes.

[1] K. F. Kelton, *Solid State Physics* (Academic, New York, 1991), Vol. 45, pp. 75–90.
[2] D. Kashchiev, *Nucleation: Basic Theory with Applications* (Butterworth-Heinemann, Oxford, 2000).
[3] P. G. Vekilov, Soft Matter **6**, 5254 (2010).
[4] M. Volmer and A. Weber, Z. Phys. Chem. **119**, 277 (1926).
[5] L. Farkas, Z. Phys. Chem. **125**, 239 (1927).
[6] R. Becker and W. Döring, Ann. Phys. **416**, 719 (1935).
[7] See, e.g., C. K. Bagdassarian and D. W. Oxtoby, J. Chem. Phys. **100**, 2139 (1994).
[8] S. Prestipino, A. Laio, and E. Tosatti, Phys. Rev. Lett. **108**, 225701 (2012).
[9] A. Dillmann and G. E. A. Meier, J. Chem. Phys. **94**, 3872 (1991).
[10] See, e.g., W. H. Shih, Z. Q. Wang, X. C. Zeng, and D. Stroud, Phys. Rev. A **35**, 2611 (1987).
[11] J. W. Cahn and J. E. Hilliard, J. Chem. Phys. **28**, 258 (1958).
[12] J. W. Cahn and J. E. Hilliard, J. Chem. Phys. **31**, 688 (1959).
[13] M. P. A. Fisher and M. Wortis, Phys. Rev. B **29**, 6252 (1984).
[14] P. Harrowell and D. W. Oxtoby, J. Chem. Phys. **80**, 1639 (1984).
[15] Y. C. Shen and D. W. Oxtoby, J. Chem. Phys. **105**, 6517 (1996).

[16]See, for example, M. Kardar, *Statistical Physics of Fields* (Cambridge University Press, 2007).

[17]B. J. Block, S. K. Das, M. Oettel, P. Virnau, and K. Binder, J. Chem. Phys. **133**, 154702 (2010).

[18]R. C. Tolman, J. Chem. Phys. **17**, 333 (1949).

[19]See, e.g., L. Filion, M. Hermes, R. Ni, and M. Dijkstra, J. Chem. Phys. **133**, 244115 (2010).

[20]T. Zykova-Timan, C. Valeriani, E. Sanz, D. Frenkel, and E. Tosatti, Phys. Rev. Lett. **100**, 036103 (2008).

[21]P. Canham, J. Theor. Biol. **26**, 61 (1970).

[22]W. Helfrich, Z. Naturforsch. C **28**, 693 (1973).

[23]H. S. Kogon and D. J. Wallace, J. Phys. A **14**, L527 (1981).

[24]K. Kassner, e-print arXiv:cond-mat/0607823.

[25]M. Napiórkowski and S. Dietrich, Phys. Rev. E **47**, 1836 (1993).

[26]J. G. Segovia-López, A. Zamora, and J. A. Santiago, J. Chem. Phys. **135**, 064102 (2011).

[27]M. Abate and F. Tovena, *Curve e superfici* (Springer Italia, Milano, 2006), Observations 5.3.21 and 5.3.22.

[28]M. Abate and F. Tovena, *Curve e superfici* (Springer Italia, Milano, 2006), Corollary 5.3.24.

[29]T. Zykova-Timan, D. Ceresoli, U. Tartaglino, and E. Tosatti, J. Chem. Phys. **123**, 164701 (2005).

[30]S. T. Milner and S. A. Safran, Phys. Rev. A **36**, 4371 (1987).

[31]N. J. Günther, D. A. Nicole, and D. J. Wallace, J. Phys. A **13**, 1755 (1980).

[32]P. R. ten Wolde and D. Frenkel, J. Chem. Phys. **109**, 9901 (1998).

[33]H. Reiss and R. K. Bowles, J. Chem. Phys. **111**, 7501 (1999).

[34]R. K. Bowles, R. McGraw, P. Schaaf, B. Senger, J.-C. Voegel, and H. Reiss, J. Chem. Phys. **113**, 4524 (2000).

[35]L. Maibaum, Phys. Rev. Lett. **101**, 019601 (2008).

[36]A. C. Pan and D. Chandler, J. Phys. Chem. B **108**, 19681 (2004).

[37]L. D. Gelb, J. Chem. Phys. **118**, 7747 (2003).

[38]K. K. Mon, S. Wansleben, D. P. Landau, and K. Binder, Phys. Rev. B **39**, 7089 (1989).

[39]M. Hasenbusch and K. Pinn, Physica A **192**, 342 (1993).

[40]C. Rottman and M. Wortis, Phys. Rev. B **29**, 328 (1984).

[41]M. Hasenbusch and K. Pinn, J. Phys. A **30**, 63 (1997).

[42]J. Hoshen and R. Kopelman, Phys. Rev. B **14**, 3438 (1976).

[43]H. Müller-Krumbhaar, Phys. Lett. A **50**, 27 (1974).

[44]G. Wulff, Z. Kristallogr. **34**, 449 (1901).

[45]W. K. Burton, N. Cabrera, and F. C. Frank, Philos. Trans. R. Soc. London, Ser. A **243**, 299 (1951).

[46]T. Li, D. Donadio, and G. Galli, J. Chem. Phys. **131**, 224519 (2009).

[47]T. Li, D. Donadio, G. Russo, and G. Galli, Phys. Chem. Chem. Phys. **13**, 19807 (2011).

[48]M. Franke, A. Lederer, and H. J. Schöpe, Soft Matter **7**, 11267 (2011).